MINISTRY OF EDUCATION

THE ANNALS OF "DUNAREA DE JOS" UNIVERSITY OF GALATI

Fascicle IX
METALLURGY AND MATERIALS SCIENCE

YEAR XLI (XLVI)
June 2023, no. 2

ISSN 2668-4748; e-ISSN 2668-4756

2023
GALATI UNIVERSITY PRESS

EDITORIAL BOARD

THE ANNALS OF "DUNAREA DE JOS" UNIVERSITY OF GALATI
FASCICLE IX. METALLURGY AND MATERIALS SCIENCE
Nº. 2 - 2023, ISSN 2668-4748; e-ISSN 2668-4756
Volume DOI: https://doi.org/10.35219/mms.2023.2

Table of Contents

THE ANNALS OF "DUNAREA DE JOS" UNIVERSITY OF GALATI
FASCICLE IX. METALLURGY AND MATERIALS SCIENCE
Nº. 2 - 2023, ISSN 2668-4748; e-ISSN 2668-4756
Volume DOI: https://doi.org/10.35219/mms.2023.2

THE ANNALS OF "DUNAREA DE JOS" UNIVERSITY OF GALATI
FASCICLE IX. METALLURGY AND MATERIALS SCIENCE
Nº. 2 - 2023, ISSN 2668-4748; e-ISSN 2668-4756
Article DOI: https://doi.org/10.35219/mms.2023.2.01

RESEARCH ON OBTAINING SINTERED MATERIALS FROM 410 STAINLESS STEEL POWDER

Simona BOICIUC
"Dunarea de Jos" University of Galati, Romania
e-mail: simona_boiciuc@yahoo.com

ABSTRACT

Ferritic steels are used in applications that require good thermal conductivity and/or durability in operation involving heat cycles. They are easy to process due to their high ductility and have magnetic properties.

The paper presents a series of experimental research on the manufacture of sintered products obtained from 410 stainless steel powder and their characterization from the microstructural and wear resistance point of view.

KEYWORDS: powder metallurgy, 410 stainless steel, abrasive wear

1. Introduction

The development of powder metallurgy was determined by the need to obtain products with special properties.

Special attention was paid to the development of corrosion-resistant sintered steel with a ferritic structure. Due to the rich content of chromium and the presence of chromium oxides on the granules surface, a series of difficulties arise during sintering, so that in order to obtain compact and resistant materials one needs sintering temperatures higher than those for ordinary ferrous materials. In the case of simple pressing and sintering, liquid phase sintering can be applied in order to achieve high compactness. However, the high contraction during sintering leads to the need for subsequent splintering processing [1-6].

Stainless steels are used in various industrial branches due to their high resistance to corrosion in the atmosphere, water vapor, aqueous solutions of salts of organic acids and nitric acid.

The corrosion resistance of low-alloy steels is quite reduced, because the oxides formed do not provide a sufficiently compact structure to protect the alloy from chemical interaction with the corrosive environment. By increasing the chromium content to 12%, the oxidation potential of Fe-Cr alloys changes suddenly, increasing from -0.6 V to 0.2 V, thus becoming positive and ensuring the necessary structure for exploitation in corrosive environments [1-6].

The 410 ferritic stainless steels are characterized by resistance to atmospheric corrosion, sea water and resistance in a series of acids, salts, alkalis, by a high plasticity, heat stability, resistance to thermal shocks and to medium pressures, so they are used in the production of guide parts, pinions, ABS sensors, valves, components for steam and hydraulic turbines, household appliances, in the food and medical industries [1-6].

The 410 stainless steel powder is easy to process and has a corrosion resistance superior to martensitic and a lower cost price than austenitic.

In this paper, the aim is to obtain certain products from stainless steel powder 410, through specific technologies of powder metallurgy and their characterization from the point of view of microstructure and wear resistance.

2. Experimental conditions

In order to obtain the sintered products, a 410 ferritic stainless-steel powder (X12Cr13, SR EN 10088-2:1998) was used with the following chemical composition: 0.15%C; 13.5%Cr; 0.8%Si; 0.2% Mn; 0.015%S; 0.035% P; rest Fe.

The powders were cold-pressed, using the universal machine for mechanical tests. The pressures used to compact the 410 powder were 540, 628, 726, 863 MPa. The compressed samples are cylindrical in shape with dimensions of approximately 8 X 6 mm.

The sintering of compressed items from 410 powders was carried out in a laboratory furnace. The samples were placed in a ceramic cylinder, in which graphite was added. It prevents the penetration of air, thus ensuring the protective atmosphere.

THE ANNALS OF "DUNAREA DE JOS" UNIVERSITY OF GALATI
FASCICLE IX. METALLURGY AND MATERIALS SCIENCE
No. 2 - 2023, ISSN 2668-4748; e-ISSN 2668-4756
Article DOI: https://doi.org/10.35219/mms.2023.2.01

Sintering was performed at a temperature of 1150 °C, for 60 minutes, and cooling was done along with the furnace.

The microscopic analysis of the sintered samples was performed with a Neophot 2 microscope with computer data acquisition.

The microhardness HV 0.05 determined on the sintered powder compressed items was performed on a PMT-3 micro-durimeter, with a load of 50 g.

The porosity of the compressed items was determined by the method of linear segments.

The 410 stainless steel sintered samples were subjected to wear testing on a rotating disc with sandpaper. The method consists in successively pressing, under identical conditions, the powder compressed items, 8 x 6 mm in size, on a rotating disk, covered with sandpaper with a 120 grit. A mechanism for radial movement of the sample by 0.5 mm/rot ensures spiral travel on the surface of the rotating disc. A device for applying a 6.229 N load ensures the perpendicular pressing of the test piece on the sandpaper at the pressure of 0.123 N/mm^2. At the disk speed of 25 rpm, a road length of 11.6 m was covered.

3. Experimental results

Following the microscopic analysis, carried out on the 410 ferritic stainless-steel powder and shown in Figure 1, it was found that it has an irregular shape specific to atomization in water, being suitable for mould formation and sintering in order to obtain products with high compactness.

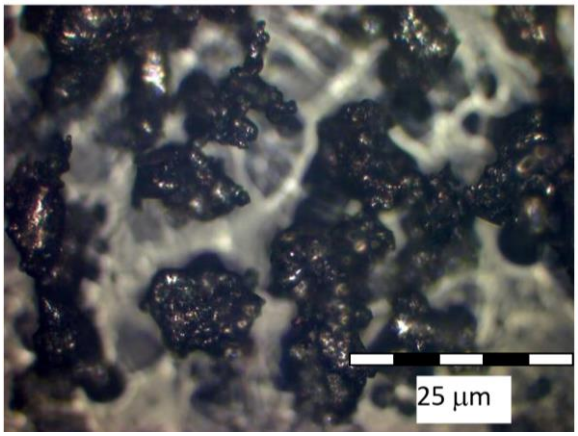

Fig. 1. *Aspect of 410 stainless steel powder*

The microstructure of the 410 ferritic stainless-steel powder, shown in Figure 2, is composed of alloyed ferrite and was highlighted by metallographic etching with 2% nital.

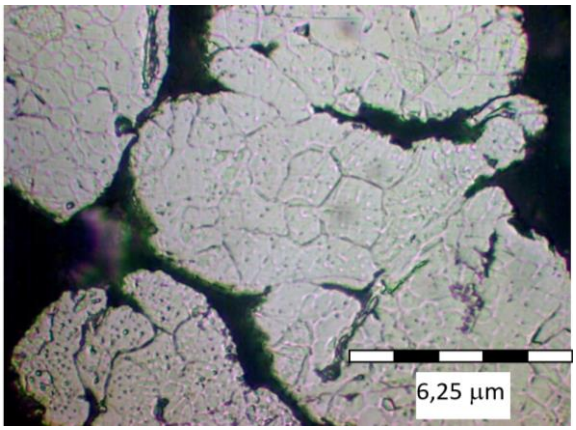

Fig. 2. *Microstructure of 410 ferritic stainless-steel powder, nital attack 2%*

The microhardness of the powder determined on the polished section of the particles under the load of 50 g was HV 0.05 = 2309.5 MPa.

Figure 3 shows the metallographic aspect of the powder compressed items, cold-formed with different pressures. It can be seen that with the increase in pressure there is a reduction in porosity and an increase in the mechanical cohesion between the particles.

The cold-pressed samples show low mechanical and physical properties due to the presence of intercommunicating pores, crystalline defects and internal stresses in the deformed particles. That is why the sintering operation is necessary.

Sintering involves a thermally activated mass transport process that leads to the strengthening of bonds between particles and/or to the modification of porosity and pore geometry and to the reduction of the free energy of the system (by reducing the free surface).

The microscopic analysis carried out on the pressed and sintered samples in an unatacked state, and presented in Figure 4, highlighted the fact that after sintering there is an increase in the mechanical resistance of the contact sections between the particles and a reduction in porosity (the pores in the material round off and the small ones disappear in the favour of the big ones). These phenomena increase in intensity with the increase of the forming pressure from 540 MPa to 863 MPa.

THE ANNALS OF "DUNAREA DE JOS" UNIVERSITY OF GALATI
FASCICLE IX. METALLURGY AND MATERIALS SCIENCE
No. 2 - 2023, ISSN 2668-4748; e-ISSN 2668-4756
Article DOI: https://doi.org/10.35219/mms.2023.2.01

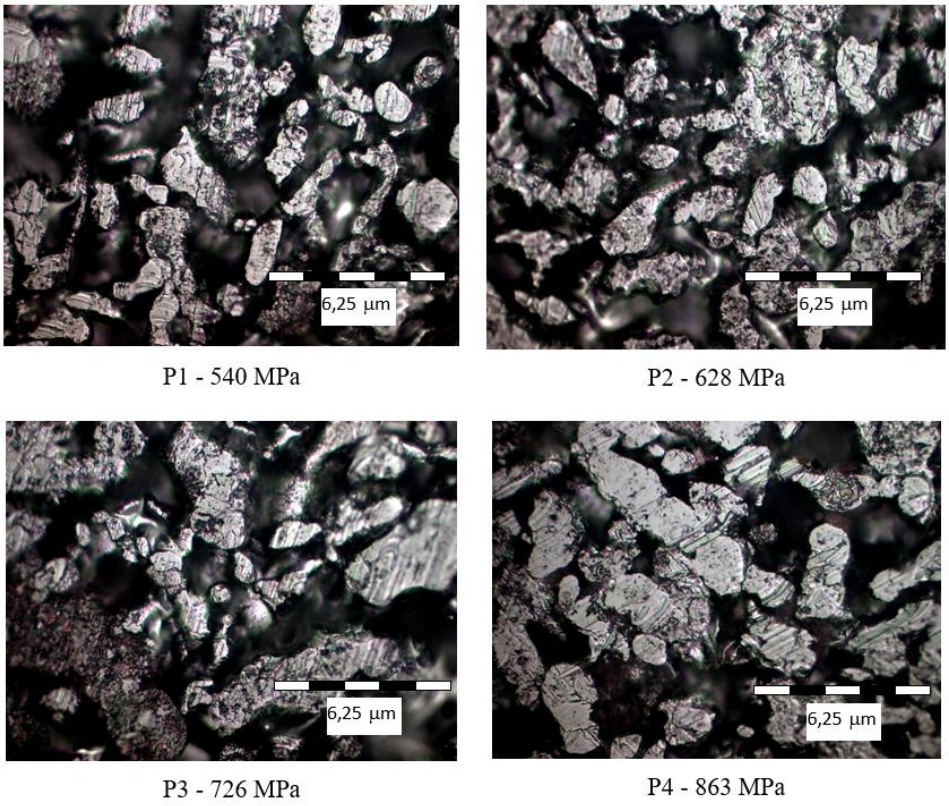

Fig. 3. *Metallographic aspect of 410 ferritic stainless-steel powder at different pressures*

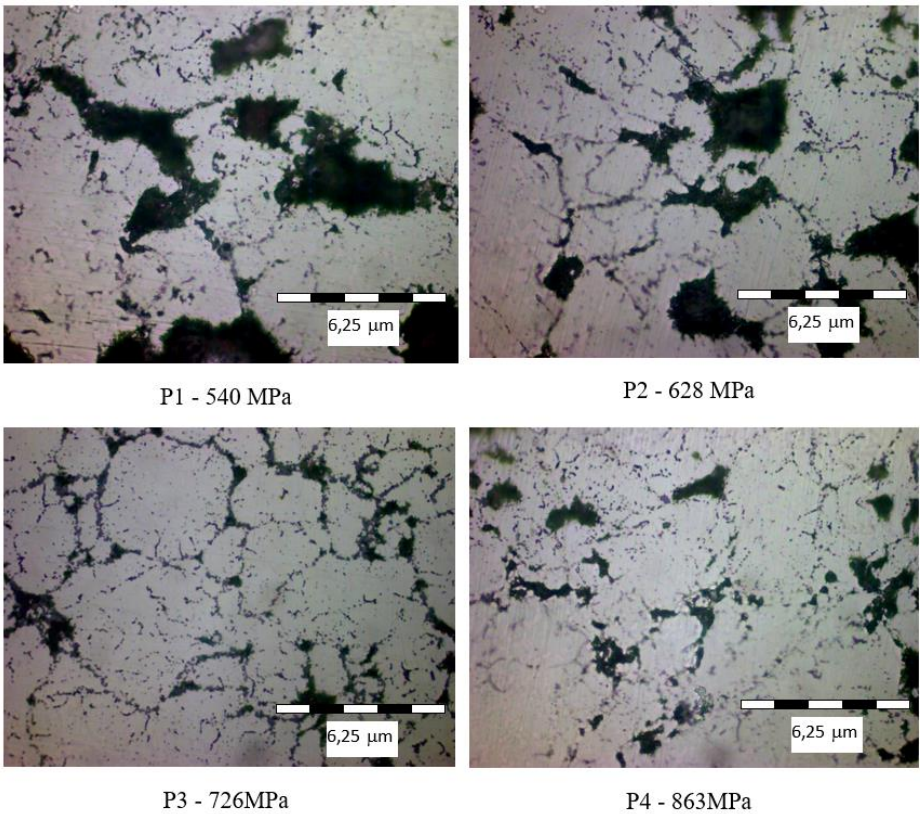

Fig. 4. *Microstructure of sintered 410 ferritic steel samples, unattacked state*

THE ANNALS OF "DUNAREA DE JOS" UNIVERSITY OF GALATI
FASCICLE IX. METALLURGY AND MATERIALS SCIENCE
Nº. 2 - 2023, ISSN 2668-4748; e-ISSN 2668-4756
Article DOI: https://doi.org/10.35219/mms.2023.2.01

Analysing Figure 5, it can be seen that the structure of the 410 ferritic stainless-steel samples in the sintered state and attacked with nital 2% is formed by ferrite and carbides. The presence of carbides is due to the sintering medium used, namely graphite.

The microhardness HV 0.05 determined on the sintered powder compressed items was HV 0.05 = 6222.3 MPa, superior to the powder in its initial state.

Increasing the duration and temperature of sintering can lead to an increase in grain size with direct implications on strength and ductility.

The porosity of the samples was determined by the method of linear segments. Analysing Figure 6, it results that as the formation pressure increases, the porosity decreases. It varies between 0.35-0.24 at the edge of the compressed items and between 0.48-0.28 in their centre.

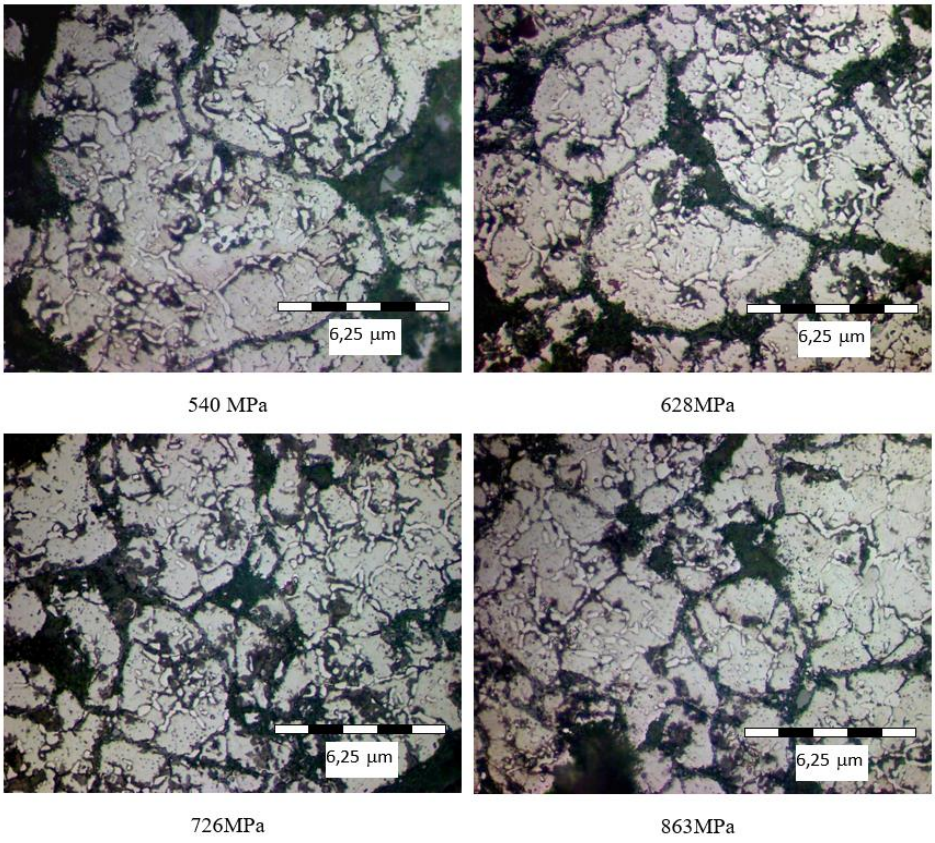

Fig. 5. *Microstructure of sintered 410 ferritic stainless-steel samples, nital attack 2%*

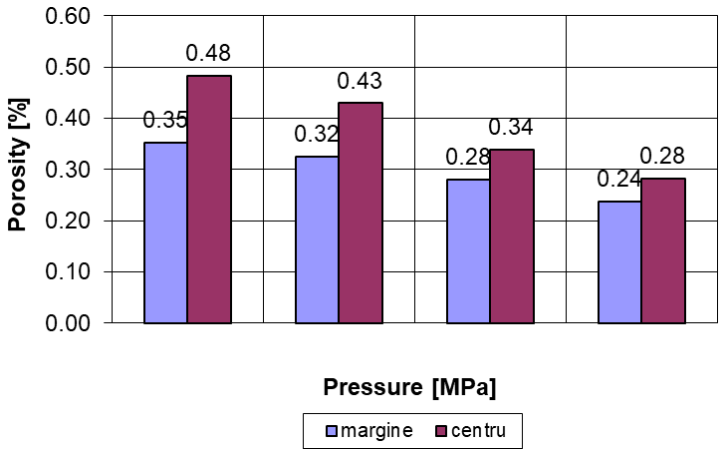

Fig. 6. *Porosity variation with formation pressure*

THE ANNALS OF "DUNAREA DE JOS" UNIVERSITY OF GALATI
FASCICLE IX. METALLURGY AND MATERIALS SCIENCE
No. 2 - 2023, ISSN 2668-4748; e-ISSN 2668-4756
Article DOI: https://doi.org/10.35219/mms.2023.2.01

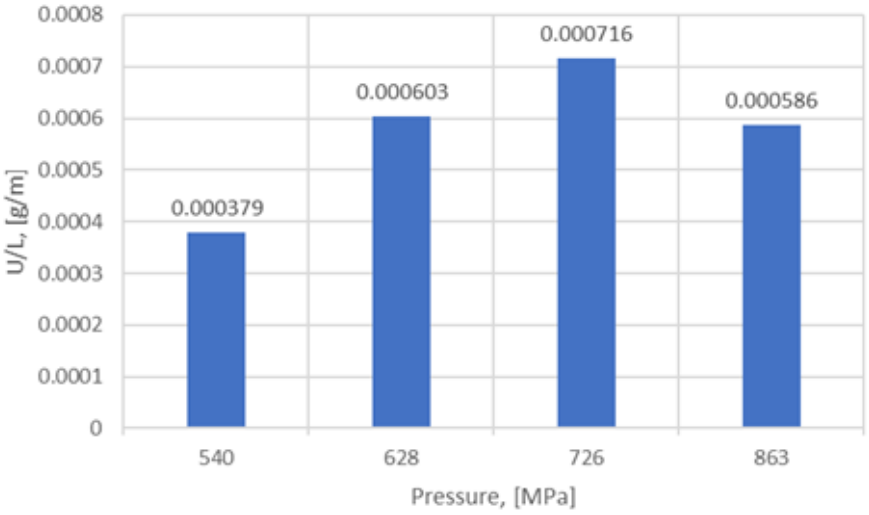

Fig. 7. *Abrasive wear behaviour of sintered powder products*

The samples thus obtained were subjected to the wear test on a rotating disk with sanding paper.

The results obtained are presented in Figure 7.

The 410 stainless steel powder is recommended to be pressed at lower pressures of about 540 MPa to ensure superior wear resistance. Pressing at low pressures causes a higher porosity which probably favours the carburization of the samples leading to an increase in wear resistance.

4. Conclusions

Obtaining products from 410 ferritic stainless-steel powders highlighted the following:

- the powder used in the experimental research has an irregular shape specific to atomization in water, with a structure made of alloyed ferrite;
- compacting the powder was achieved at pressures of 540, 628, 726, 863 MPa; it was found that when the pressure increases, the porosity of the compressed items decreases and the mechanical cohesion between the particles increases;
- sintering the powder compressed items at 1150 ^{o}C for one hour led to the reduction of their porosity and the strengthening of the bonds between the particles; the microstructure of the samples consists of ferrite and carbides;
- the microhardness HV 0.05 determined on the sintered powder compressed items was HV 0.05 = 6222.3 MPa superior to the powder in its initial state HV 0.05 = 2309.5 MPa; the increase in hardness was due to the presence of carbides; in this case, a decrease in corrosion resistance can be observed;
- as for the wear resistance on the abrasive disc, it was found that the 410 stainless steel powder is recommended to be pressed at lower pressures of about 540 MPa to ensure superior wear resistance;
- pressing at high pressures leads to higher compaction which provides poorer hardening.

References

[1]. Geru N., *Physical metallurgy (Metalurgie fizică)*, Didactic and Pedagogical Publishing House, Bucharest, 1981.
[2]. Rădulescu M., *Study of metals (Studiul Metalelor)*, Didactic and Pedagogical Publishing House, Bucharest, 1982.
[3]. Domşa A., *et al.*, *Technology of manufacturing parts from metal powders (Tehnologia fabricării pieselor din pulberi metalice)*, Technical Publishing House, Bucharest, 1966.
[4]. Palfalvi A., *Powder Metallurgy (Metalurgia Pulberilor)*, Technical Publishing House, Bucharest, 1988.
[5]. Surdeanu T., Perneş M., *Parts sintered from metal powders (Piese sinterizate din pulberi metalice)*, Technical Publishing House, Bucharest, 1984.
[6]. ***, *Stainless Steels – ASM Specialty Handbook*, 2004.

THE ANNALS OF "DUNAREA DE JOS" UNIVERSITY OF GALATI
FASCICLE IX. METALLURGY AND MATERIALS SCIENCE
No. 2 - 2023, ISSN 2668-4748; e-ISSN 2668-4756
Article DOI: https://doi.org/10.35219/mms.2023.2.02

RESEARCH ON THE RICE BRAN OIL – FLAMMABILITY TESTS ON A HIGH TEMPERATURE SURFACE

Liviu Cătălin ȘOLEA, Romică CREȚU
"Dunarea de Jos" University of Galati, Romania
e-mail: csolea@ugal.ro

ABSTRACT

In this work rice oil was tested when it is dripped onto a high temperature surface. The tests conducted determined the lowest temperature at which rice oil ignited and the highest temperature at which rice oil did not ignite in three tests conducted at the same temperature. The results of this study show that the values of the evaluated temperatures are of major importance regarding the use of rice oil as an eco-friendly lubricant. Thus, the highest temperature at which rice oil did not ignites is 465 °C, while the lowest temperature at which rice oil ignited is 470 °C. Moreover, at the end of the 8 tests performed, part of the oils collected in the tray of the installations used in the present study were subjected to spectrophotometric tests. Based on the obtained data, the transmittance spectra were plotted and the trichromatic components and coordinates were calculated, as well as the colour differences of the tested oils.

KEYWORDS: rice bran oil, flammability, CIELAB, chromatic coordinates, colour differences, eco-friendly lubricant

1. Introduction

Flammable liquids and gases, as well as concentrations of solid or liquid particles dispersed in a gaseous medium, can randomly interact with a high-temperature surface and ignite, causing major damage to the installations in which they operate. That is why it is necessary to know with as much probability as possible the maximum temperature at which flammability does not occur, as well as the lowest temperature at which flammability occurs for the sources listed above.

A number of researchers have studied the phenomena that determine the flammability of various liquids and gaseous media on surfaces with high temperatures [1-11]. In his studies, Babrauskas [12] listed and analysed methods for investigating the flammability of liquids, gases, and vapours on high-temperature surfaces. On the other hand, a series of scientific papers [13-15] analysed the flammability on hot surfaces of various types of vegetable oils. Also, in the last period of time, a series of tribological and rheological studies were carried out on rice bran oils, this being considered a potential ecological lubricant [16-21]. The use of bio-lubricants is increasingly recommended [20], especially in the context where recent research [22] shows that under the conditions of forestry strategies, for example, it is necessary to minimize the inevitable effects of anthropogenic climate changes in the future.

2. Experimental results

The flammability tests on a heated surface, for rice oil, were carried out on an installation belonging to the lubricant analysis laboratory of the Faculty of Engineering from "Dunarea de Jos" University of Galați.

The setup and working procedures have been extensively described in [9, 13, 14]. On the surface of the cylinder (Fig. 1), heated to various temperatures, a quantity of 10 ± 0.5 mL of rice oil is dripped, the draining time being 50 ± 5 sec. During the entire test period the temperature of the cylinder remains constant.

Analysing the flammability tests performed by various authors [9-15] for a series of vegetable, mineral and synthetic oils, it resulted that the first temperature test of rice oil should be performed at the temperature of 480 °C.

According to our studies, the test conducted showed that the rice oil ignited after 11 seconds after starting the test (Fig. 1.b). From the first drops that

THE ANNALS OF "DUNAREA DE JOS" UNIVERSITY OF GALATI
FASCICLE IX. METALLURGY AND MATERIALS SCIENCE
Nº. 2 - 2023, ISSN 2668-4748; e-ISSN 2668-4756
Article DOI: https://doi.org/10.35219/mms.2023.2.02

come into contact with the heated cylinder, a lot of smoke is released.

In Figure 1.c (second 21 of the test) the most intense burning of the oil during the test can be seen. It was also observed that the oil continued to burn on the cylinder surface for another 7 seconds after the test ended (Fig. 1.d).

The test temperature was then decreased by 30 °C. The test performed at a temperature of 450 °C established that the oil does not ignite throughout the test (Fig. 2.a), the amount of smoke released when the oil comes into contact with the heated cylinder is insignificant compared to the tests that followed.

a) 1st second *b) 11th second*

c) 21st second *d) 62nd second*

***Fig. 1.** Rice oil tested at 480 °C*

Under these conditions, the next test was performed at a temperature located in the middle of the range between the temperatures of 450 °C and 480 °C, this temperature being 465 °C. The experimental results showed that even at this temperature the rice oil did not ignite, throughout the test (Fig. 2.b). This is the first test at a temperature of 465 °C at which the rice oil did not ignite.

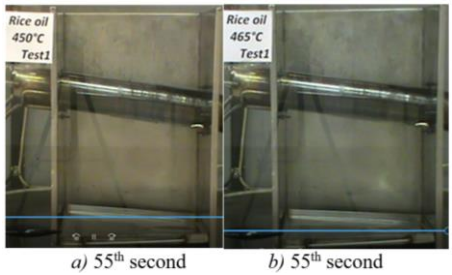

a) 55th second *b)* 55th second

***Fig. 2.** Rice oil tested at 450 °C – test 1 (a) and 465 °C – test 1 (b)*

In order to achieve the proposed objective, the oil was tested at a temperature of 475 °C, a temperature located approximately in the middle of the range 465-480 °C. At this test temperature the oil ignited after 21 seconds from the start of the test (Fig. 3.b). Figure 3.c (second 29 of the test) showed the most intense oil burning during the test. And in this case the oil continues to burn, on the surface of the cylinder, after the test has ended (Fig. 3.d), the burning time being 5 seconds (a time shorter than that recorded in the case of the oil tested at a temperature of 480 °C).

The next test was performed at the next temperature at which the rice oil did not ignite, this temperature being 465 °C. At this temperature, two consecutive tests were performed in which the tested oil did not ignite (Fig. 4).

Thus, the highest temperature (465 °C) at which rice oil does not ignite was established (a total of 3 tests were performed at a temperature of 465 °C where the oil did not ignite) and the lowest temperature (475 °C) in which rice oil ignite.

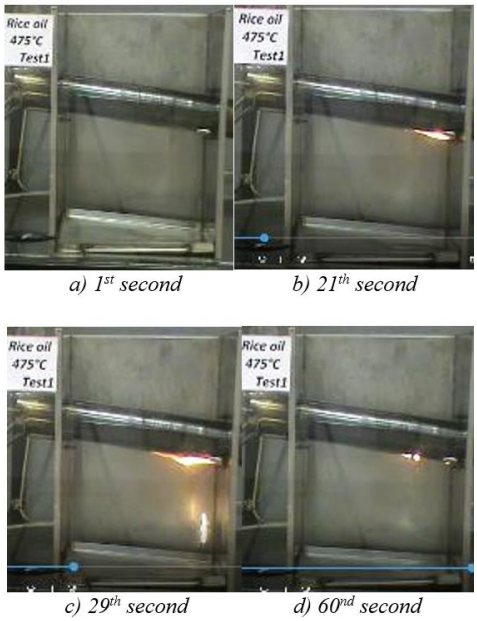

a) 1st second *b) 21th second*

c) 29th second *d) 60nd second*

***Fig. 3.** Rice oil tested at 475 °C*

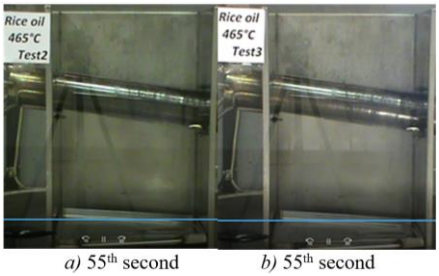

a) 55th second *b)* 55th second

***Fig. 4.** Rice oil tested at 465 °C, test 2 (a) and 465 °C, test 3 (b)*

THE ANNALS OF "DUNAREA DE JOS" UNIVERSITY OF GALATI
FASCICLE IX. METALLURGY AND MATERIALS SCIENCE
Nº. 2 - 2023, ISSN 2668-4748; e-ISSN 2668-4756
Article DOI: https://doi.org/10.35219/mms.2023.2.02

Fig. 5. *Rice oil tested at 470 °C, test 1-55th second*

In order to refine the range between the two temperatures, it was decided to carry out a maximum of three more tests halfway between the two temperatures specified above. Thus, tests were carried out at a temperature of 470 °C. The first test performed at the temperature mentioned above revealed that rice oil does not inflame (Fig. 5).

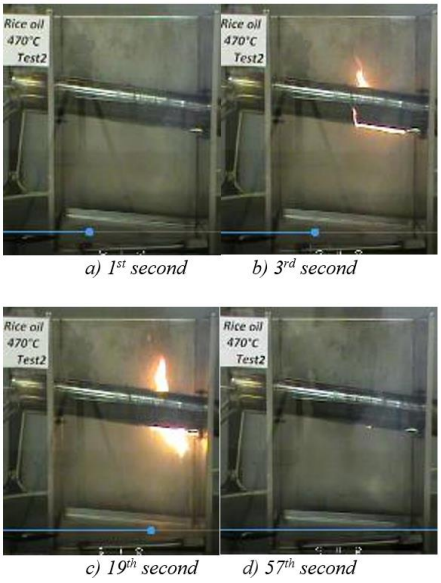

a) 1st second *b) 3rd second*

c) 19th second *d) 57th second*

Fig. 6. *Rice oil tested at 470 °C, test 2*

In the case of the second test performed at a temperature of 470 °C, the oil ignites after only 3 seconds from the start of the test (Fig. 6.b). According to Figure 6.c (second 19 of the test) the most intense burning of the oil during the test was identified. And in this case the oil continues to burn, on the surface of the cylinder, after the test is over (Fig. 6.d). The burning time was only 2 seconds (a time shorter than that recorded in the case of the oil tested at a temperature of 475 °C).

The lowest temperature at which rice oil ignites is 470 °C, and the highest temperature at which rice oil does not ignite (after 3 tests) is 465 °C.

Figure 7 shows the order and results of the 8 tests performed.

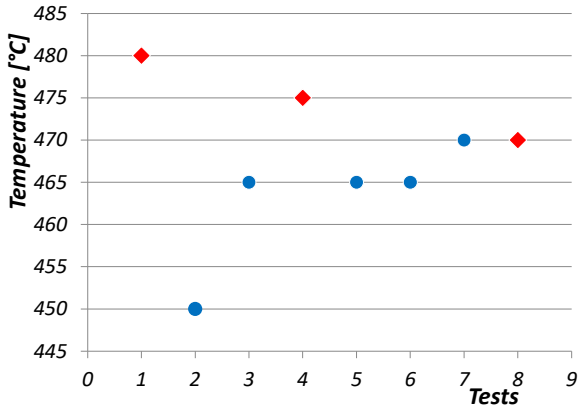

Fig. 7. *Flammability tests for rice oil (the red rhombus – it ignites; the blue circles – it does not ignite)*

At the end of the 8 tests carried out, part of the oils collected in the tray of the installation were subjected to spectrophotometric tests. Thus, the transmittance curves of the untested rice oil, as well as of the samples where the rice oil was tested at the temperature of 470 °C (test 1 – the oil does not burn and test 2 – the oil burns) and for the tested oil were determined at a temperature of 465 °C (test 1 – the oil does not burn).

Transmittance values were determined in the wavelength range of 380-780 nm, using a measurement step of 0.2 nm. A 10 mm glass cuvette was used.

Figure 8 shows the transmittance curves of the oils tested at temperatures of 465 °C (test 1 - the oil did not burn), 470 °C (test 1 - the oil did not burn), 470 °C (test 2 - the oil burned) as well as for untested rice oil.

Based on the experimental values of the transmittances determined at the wavelengths of 445, 495, 550 and 625 nm, the trichromatic components and coordinates were calculated (Table 1), these being the calculation support for determining the chromatic coordinates (Table 2) and the colour differences (Table 3) for the oil samples tested at the above-mentioned temperatures as well as for the untested rice oil.

From the analysis of the transmittance curves (Fig. 8), very small differences can be observed between the oil that was not tested for flammability and the oils that did not ignite at the temperatures of 465 °C and 470 °C, respectively test 1.

THE ANNALS OF "DUNAREA DE JOS" UNIVERSITY OF GALATI
FASCICLE IX. METALLURGY AND MATERIALS SCIENCE
No. 2 - 2023, ISSN 2668-4748; e-ISSN 2668-4756
Article DOI: https://doi.org/10.35219/mms.2023.2.02

On the other hand, a major difference is observed between the case of the oil that ignited at the temperature of 470 °C (test 2) and the untested oil. This is due to the radical chemical transformations through which the lipids and other organic molecules in the oil composition undergo as the working temperature increases, also studied in our recent research [23].

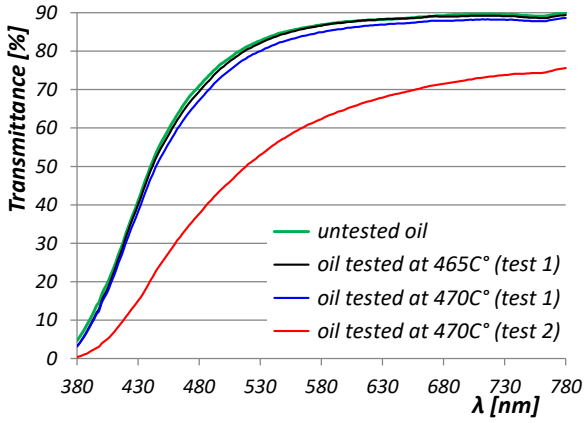

Fig. 8. *Spectral transmittance curves of rice oils*

Moreover, as can be seen from table 1, these chemical transformations that occur with the change in temperature induce, at the same time, chromatic variations in accordance with the conditions of the tests carried out. Thus, both in the case of the trichromatic components and that of the trichromatic coordinates, the variations of these parameters are noted depending on the temperature at which the flammability tests were performed.

These results are highlighted in the case of the oil tested at the temperature of 470 °C (the oil burns) when the location of the colour of the oil in the chromatic circle is totally different from that of the untested oil.

This shows that, at this temperature, the behavior of the oil is different when performing the two tests, consistent with the fact that the chromophore and auxochrome groups undergo transformations in turn. This aspect is much more relevant in the case of expressing the colour variation of oil subjected to flammability tests by means of the chromatic coordinates L^*, a^*, b^*, respectively C^*_{ab} and h_{ab} (Table 2).

Table 1. *Experimental results for rice oils tested at various temperatures, obtained according to the color system (x, y) CIE 1964 (CIEXYZ)/Illuminant D65/10°*

Rice oils	*Trichromatic components*			*Trichromatic coordinates*		
	X	***Y***	***Z***	***x***	***y***	***z***
Untested oil	*78.029*	*80.299*	*68.682*	*0.344*	*0.354*	*0.303*
Oil tested at 465 °C (test 1)	*77.613*	*79.782*	*67.231*	*0.346*	*0.355*	*0.299*
Oil tested at 470 °C (test 1)	*75.919*	*77.941*	*64.611*	*0.348*	*0.357*	*0.296*
Oil tested at 470 °C (test 2)	*53.270*	*53.572*	*31.952*	*0.384*	*0.386*	*0.230*

Table 2. *Chromatic coordinates (CIELAB system) for rice oils tested at various temperatures/ Illuminant D65/10°*

Rice oils	*Chromatic coordinates*			***a^*/b^****	***$(a^*/b^*)^2$***	***C^*_{ab}***	***h_{ab}***
	L^*	***a^****	***b^****				
Untested oil	*91.82*	*3.83*	*13.53*	*0.28*	*0.08*	*14.06*	*74.21*
Oil tested at 465 °C (test 1)	*91.59*	*3.99*	*14.36*	*0.28*	*0.08*	*14.90*	*74.46*
Oil tested at 470 °C (test 1)	*90.75*	*4.16*	*15.17*	*0.27*	*0.0752*	*15.73*	*74.67*
Oil tested at 470 °C (test 2)	*78.21*	*6.50*	*28.88*	*0.23*	*0.051*	*29.60*	*77.32*

Our results show that by decreasing the brightness parameter of the tested oil by 14.82%, it is evident that the colour of the tested oil darkens as its temperature approaches the point where the oil burns. This is due to the effect of decreasing light absorption intensity as the temperature of the oil approaches the ignition point.

At the same time, the yellowness parameter increases as the test temperature is higher. Thus, the colour coordinate b* increases from 13.53, value corresponding to the standard oil, to 14.36 which corresponds to the first test of the oil at a temperature of 465 °C, respectively the highest temperature at which the rice oil did not ignite.

Moreover, the yellowness parameter value increases to 15.17 when the test temperature becomes 470 °C. According to the data in Table 2, the increase by more than 50% compared to the untested oil sample is highlighted, when the test temperature becomes 470 °C and the oil burns.

THE ANNALS OF "DUNAREA DE JOS" UNIVERSITY OF GALATI
FASCICLE IX. METALLURGY AND MATERIALS SCIENCE
No. 2 - 2023, ISSN 2668-4748; e-ISSN 2668-4756
Article DOI: https://doi.org/10.35219/mms.2023.2.02

Relatively large differences in the variation of the yellowness parameter also resulted between the two tests (test 1 versus test 2) carried out on rice oil at the same temperature, respectively 470 °C. If in the case of test 1 the increase in the yellowness parameter is approximately 12% (variation by 1.64 units), in the case of test 2 this variation is more than 15 units (Table 3).

This shows that at the burning temperature the degree of yellowness is intensified compared to the condition where the oil is not burning, although the test temperature is the same. This is probably due to the organic compounds formed, such as hydroperoxides, during the heating of the tested oil.

Also, the data presented in Table 2 indicate a similar variation in the case of chroma, the rice oil subjected to test 2 at the temperature of 470 °C presenting the highest value of this chromatic parameter. The much higher value proves the superior colour intensity of the rice oil subjected to test 2 compared to that subjected to test 1, although the test temperature is the same.

The highest temperature at which the rice oil did not ignite, namely 465 °C, also corresponds to the lower values (14.9 and 74.46) of the chroma parameters, C^*_{ab}, respectively the hue angle, h_{ab}. Moreover, the colour variation, ΔE^*_{ab} [24] correlates directly with the test temperature at which rice oil burns (Table 3).

Table 3. *Experimental values of colour differences for rice oils tested at various temperatures*

Rice oils	ΔL^*	Δa^*	Δb^*	ΔC^*_{ab}	Δh_{ab}	ΔE^*_{ab}
Oil tested at 465 °C (test 1)	*-0.23*	*0.16*	*0.83*	*0.84*	*0.25*	*0.88*
Oil tested at 470 °C (test 1)	*-1.07*	*0.33*	*1.64*	*1.67*	*0.46*	*1.99*
Oil tested at 470 °C (test 2)	*-13.61*	*2.67*	*15.35*	*15.54*	*3.11*	*20.69*

3. Conclusions

Determining the minimum ignition point on a heated cylindrical surface of rice oil required 8 tests. For all tests in which the rice oil did not ignite (except for the oil tested at 450 °C) considerable smoke when the oil came into contact with the heated surface of the cylinder was observed.

In the case of tests where oil ignition has occurred, it is extinguished on contact with the surface of the oil pan (the oil does not sustain combustion in the pan). Oil burning on the surface of the heated cylinder continues even after the tests are finished, the recorded time varying between 7 seconds (at a temperature of 480 °C – test 1) and 2 seconds (at a temperature of 470 °C – test 2).

The maximum temperature at which rice oil does not ignite on a heated cylindrical surface is 465 °C.

The minimum temperature at which rice oil ignites on the hot surface is 470 °C.

The temperature of 470 °C keeps the oil burning to a very small extent after the test is over.

The highest temperature at which rice oil does not ignite corresponds to its maximum brightness parameter, respectively to a minimum chroma intensity. Increasing the test temperature by 5 °C leads to a decrease in brightness parameter, respectively a shift of the hue angle towards the second quadrant of the colour circle diagram, as well as an increase in chroma.

References

[1]. Colwell J. D., Reza A., *Hot surface ignition of automotive and aviation fluids*, Fire Technology, 41, p. 105-123, 2005.
[2]. Goyal V., Carayon A. B., Meyer S., Gore J., Simmons R., *Hot surface ignition temperatures of hydrocarbon fuels*, AIAA SciTech Forum, 55th AIAA Aerospace Sciences Mtg, Grapevine TX, 2017.
[3]. Shaw A., Epling W., McKenna C., Weckman E., *Evaluation of the ignition of diesel fuels on hot surfaces*, Fire Technol 46, p. 407-423, 2010.
[4]. Dillard L. N., Ulcay M. S., Gore J. P., *Effects of pressure on minimum hot surface ignition temperatures (MHSIT) in hot air crossflows*, AIAA scitech 2021 forum (AISS 2021–1346), AIAA, Combustors IV, 2021.
[5]. LaPointe N. R., Adams C. T., Washington J., *Autoignition of gasoline on hot surfaces*, Fire Arson Investig., 56(2), p. 18-21, 2005.
[6]. Haussmann G. J., Matta L. M., *Flammable vapor ignition by engine exhaust systems*, Journal of Applied Fire Science, 11, p. 335-348, 2002.
[7]. Imamura T., Uehara K., Nakata K., Maruyama S., Kuwana K., *Quas-steady characteristics of flowing propane/air mixture ignited by a heated surface*, Fire Safety Journal, vol. 120, 10025, 2021.
[8]. McTaggart - Cowan G., Huang J., Turcios M., Singh A., Munshi S., *Evaluation of a Hot-Surface Ignition System for a Direct-Injection of Natural Gas Engine*, Proc. ASME 2018 Internal combustion engine div. fall tech. conf., v.1 large bore engines; fuels; advanced combustion, San Diego, 2018.
[9]. Deleanu L., Buzoianu D., Rîpă M., Crăciunoiu S., Drug A., *Flammability tests on hot surfaces for industrial fluids*, The Annals of University ''Dunărea de Jos'' of Galați, Fascicle VIII, p. 22–31, 2007.
[10]. Hansen R., *Reviewing conditions on a mining vehicle for possible ignition and fire behaviour – flammable and combustible liquids, Sustainable Minerals Institute*, The University Of Queensland Australia, 2022.
[11]. Li Y. L., Wang Y. H., Lu S. X., *Ignition of the leaked diesel on a heated horizontal surface*, Fire Safety Journal, vol. 45, p. 58-68, 2010.

[12]. Babrauskas V., *Ignition of gases, vapors and liquids by hot surfaces*, Fire Technology, 58, p. 281-310, 2022.
[13]. Șolea L. C., Deleanu L., *Flammability tests on hot surface for castor oil*, Mechanical Testing and Diagnosis, ISSN 2247-9635, vol. 4, p. 24-28, 2020.
[14]. Șolea L. C., Deleanu L., *Flammability tests for hemp seed oil*, Mechanical Testing and Diagnosis, ISSN 2247-9635, vol. 2, p. 5-9, 2021.
[15]. Georgescu C., Cristea G. C., Șolea L. C., Deleanu L., Sandu I. G., *Flammability of Some Vegetal Oils on Hot Surface*, Revista de Chimie, 69, no. 3, p. 668-673, 2018.
[16]. Zhengqiang X., Fan F., Xiaodong L., Yanning L., *Preparation of an environmentally friendly emulsion-type lubricant based on crude rice bran wax*, Petroleum, 5, p.77-84, 2019.
[17]. Rajaganapathy C., Rajamurugan T. V., Dyson Bruno A., Murugapoopathi S., Armstrong M., *A study on tribological behavior of rice bran and karanja oil-based TiO_2 nano bio-fluids*, Materials Today: Proceedings, 2022.
[18]. Rubalya Valantina S., Arockia Jayalatha K., Phebee Angeline D. R., Uma S., Ashvanth B., *Synthesis and characterisation of electro-rheological property of novel eco-friendly rice bran oil and nanofluid*, Journal of Molecular Liquids, p. 256-266, 2018.
[19]. Rani S., Joy M. L., Prabhakaran Nair K., *Evaluation of physiochemical and tribological properties of rice bran oil – biodegradable and potential base stoke for industrial lubricants*, Industrial Crops and Products, 65, p. 328-333, 2015.
[20]. Panchal T. M., Patel A., Chauhan D. D., Thomas M., Jigar V. Patel J. V., *A methodological review on bio-lubricants from vegetable oil-based resources*, Renewable and Sustainable Energy Reviews, 70, p. 65-70, 2017.
[21]. Albino Antunes S., Lanza M., Hense H., *Rheological properties of rice bran (Oryza sativa L.) oils processing and soapstock residue*, Industrial Crops and Products, 46, p. 111-116, 2013.
[22]. Crișan V. E., Dincă L., Bragă C., Murariu G., Tupu E., Mocanu G. D., Drașovean R., *The Configuration of Romanian Carpathians Landscape Controls*, Volume Diversity of Picea Abies (L.) Stands, Land, 12, 406, p. 1-18, 2023.
[23]. Crețu R., Șolea L. C., *Effect of the Temperature and Oxidation Time on Some Physicochemical Characteristics of the Rice Bran Oil*, The Annals of "Dunarea De Jos" University of Galati, Fascicle IX, Metallurgy and Materials Science, Year XI (XIV) September 2022, No. 3, p. 5-10, 2022.
[24]. ***, *CIE Technical Report., Colorimetry*, 3rd ed., Publication 15, CIE Central Bureau, Vienna, 2004.

THE ANNALS OF "DUNAREA DE JOS" UNIVERSITY OF GALATI
FASCICLE IX. METALLURGY AND MATERIALS SCIENCE
N°. 2 - 2023, ISSN 2668-4748; e-ISSN 2668-4756
Article DOI: https://doi.org/10.35219/mms.2023.2.03

ADVANCED METHODS TO CHARACTERIZE THE STRUCTURAL MATERIALS OF RELIGIOUS BUILDINGS CONSTRUCTION

Kaoutar CHOUGRANI[1], Adriana Gabriela SCHIOPU[2], Mimoun CHOURAK[1]
[1]Department of civil engineering, National School of Applied Sciences, Mohammed First University Oujda, Morocco
[2]Faculty of Mechanics and Technology, University of Pitesti, Romania
e-mail: chougranikaoutar@gmail.com, gabriela.plaiasu@upit.ro, m.chourak@ump.ac.ma

ABSTRACT

The paper aims to present a bibliographic study of works on the characterization of materials, for mosques and historical minarets, using destructive methods (uniaxial compression, tension direct and indirect), and non-destructive testing (Schmidt rebound hardness, ultrasonic pulse velocity (UPV), scanning electron microscope (SEM) and X-ray diffraction (XRD) and their usefulness in the field of protection built cultural heritage. These religious buildings usually are constructed of brick masonry, stone, or/and reinforced cement concrete. Further, the form and amount of a structural defect is a function of the environment to which the structure is subjected. The different techniques used, for various construction materials, have determined the following parameters: the surface hardness, pulse velocity, structural composition, compressive strength, tensile strength and chemical composition. In general, these parameters govern the behavior under the different actions, and contribute to the strengthening and protection of the structure.

KEYWORDS: characterization, historical masonry, religious buildings, non-destructive tests, destructive tests

1. Introduction

Minarets hold great cultural significance as a part of humanity's heritage for coming generations, due to their historical and architectural value. However, over time, historical masonry minarets may experience damage from factors such as material degradation, seismic activity, differential settlement, and environmental effects [1]. The damages that masonry minarets suffer can lead to structural instabilities that can ultimately result in the destruction of the entire structure. Therefore, the safety of these religiously significant buildings must be thoroughly investigated, and a voluminous body of academic literature has been published, elucidating the intricacies of structural assessment procedures. Indeed! Destructive and non-destructive investigations are invaluable tools used to characterize the materials of these historical structures. By conducting these tests, engineers and architects can determine the necessary parameters for finite element modeling, which enables them to simulate the dynamic behavior of the structure under various conditions. Finally, this information can be used to reinforce and protect the structure, ensuring its longevity for generations to come [2]. To concretize the study, we have taken the example of several minarets which have been the subject of previous studies, which are:

1. Hacı Mahmut Mosque, which is situated in the charming town of Bolvadin, which is a part of the Afyon province in Turkey. The minaret stands independently on the north-east corner of the mosque, and boasts of an octagonal base that is almost as tall as the outer wall of the mosque itself. The minaret stands tall at an impressive height of 24.5 meters. The transition from the pulpit to the shaft is achieved through the skilful use of moldings with circular surfaces. The shaft itself is circular and extends all the way up to the balcony, which is supported by a base made up of similar moldings with circular surfaces. The balcony, in turn, is fashioned in the form of a parapet. The cylindrical comb, with a diameter smaller than the shaft, culminates in a metallic spire that adds to the allure of the minaret. Constructed using brick and stone masonry, the minaret has a total of 76 concrete boarding steps at its center, Fig. 1.

THE ANNALS OF "DUNAREA DE JOS" UNIVERSITY OF GALATI
FASCICLE IX. METALLURGY AND MATERIALS SCIENCE
N°. 2 - 2023, ISSN 2668-4748; e-ISSN 2668-4756
Article DOI: https://doi.org/10.35219/mms.2023.2.03

Fig. 1. *General view of hacı mahmut mosque* [1]

2. The Urla Kamanli Mosque, located in Urla, Izmir, Turkey, is an architectural masterpiece that has stood the test of time. Although there is no written record of the building date or the constructors, using comparative methods of architectural components in light of art history, it has been determined that this structure dates back to an era of early 14th century to mid-15th century (Erim 1995). The mosque is a member of a group of structures named Yahsi Bey Complex, which comprises a tomb, a Turkish bath, a primary school, and two fountains.

The structure has a square plan of 10 x 10 m, a wall thickness of 110 cm, and a height of 12.66 m. The dome and the window arches are brick masonry with thick mortar joints, while the walls of the structure are stone masonry with thick mortar joints and limestone. Utilizing squinches, which are brick masonry elements depicted in Figure 2, is a technique employed to achieve the seamless transition from walls to dome on the corners of historical structures.

Fig. 2. *South elevation view of the mosque* [3]

3. The Al-Omariya mosque, situated in the ancient city of Mosul on the western bank of the Tigris River, stands as a testament to the enduring legacy of Islamic architecture. Built in 1563 AD, three years after the arrival of Hajj Qassim bin Ali Al-Omari in Mosul, by order of the Ottoman Sultan Suleiman Al-Qanuni, the mosque remains one of the most esteemed places of worship in the region. The mosque's architectural splendour is further elevated by the addition of its minaret, which is located in the western wing of the courtyard. Comprised of three distinct parts, the prismatic base, with a width of 2.5 m and a height of 1.5 m, the cylindrical trunk, with a diameter of 2 m and a height of approximately 11 m, and the dome, which rises to approximately 2.5 m in height, as exemplified in Figure 3, the minaret stands tall, exceeding 23 m in height above the mosque's roof.

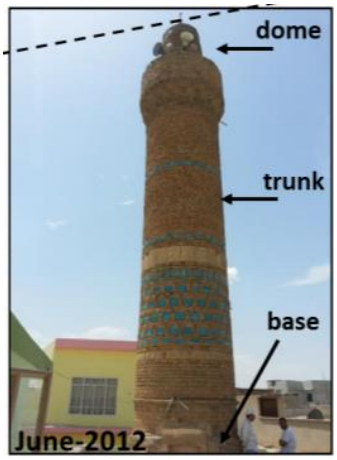

Fig. 3. *General view of Al-Omariya mosque* [4]

4. The Sütlü Minaret Mosque is an exquisite example of Ottoman architecture, characterized by a singular dome that adorns its silhouette (as depicted in Fig. 4). Situated beyond the city walls of the Battalgazi District in the City of Malatya, this mosque is steeped in historical significance. The edifice derives its name from its striking appearance, which evokes the imagery of "milky" hues. The mosque's pristine white facade, crafted from stones that retain their lustrous colour, is a testament to its enduring elegance and aesthetic appeal. The mosque is quadruple fronted and has an elevation in the west-east direction. The entry to the mosque is located on the west side facing the road.

In the initial survey, it was detected that two different types of stones were used in the construction, and the walls inside the building were completely covered with plaster. The wall is built with coursed rubble stones approximately 180 cm from the ground. The minaret of the mosque is approximately 21 m tall, and the body of the minaret has a diameter of 162 cm. The pulpit has a stone

THE ANNALS OF "DUNAREA DE JOS" UNIVERSITY OF GALATI
FASCICLE IX. METALLURGY AND MATERIALS SCIENCE
N°. 2 - 2023, ISSN 2668-4748; e-ISSN 2668-4756
Article DOI: https://doi.org/10.35219/mms.2023.2.03

coating, while the body section of the minaret was built with bricks.

Despite the absence of explicit details regarding the construction date of the Sütlü Minaret Mosque, experts have deduced that it was erected in the 16th century. This conclusion is based on the mosque's striking resemblance to the Ak Minaret Mosque, a similarly-styled edifice in the Malatya region. Over the centuries, the mosque has undergone various restorations, including a significant one in 2005 by The Directorate General of Foundations. Furthermore, an inscription on the mosque's walls bears witness to a repair work conducted in 1808.

Fig. 4. *The overall perspective of the Historical Sütlü Mosque* [5]

To accurately characterize the materials that comprise the structures, both destructive and non-destructive tests were carried out on samples of mortar, stones, and bricks that were obtained from the structures.

2. Non-destructive methods

2.1. Hardness test

To determine the surface hardness values (rebound value) of the clay brick and stone samples, for Hacı Mahmut Mosque, L and LB type Proceq Schmidt Hammers were applied. Furthermore, the Schmidt Hammer test was employed on both the stones and clay bricks that make up the intact minaret. The test results are outlined in Table 1.

The Urla Kamanli Mosque underwent a rigorous testing process to determine the strength of its stone cylinder core samples. Schmidt rebound hardness test, as per the guidelines set by the International Society for Rock Mechanics (ISRM) (1981) [6], was carried out. A steel cradle that had a cylindrical slot of the same radius as the core held the sample. A Type L Schmidt hammer, possessing an impact energy of 0.74 Nm, was utilized. A total of 37 core samples were tested, and the average results for each stone are presented in Table 1.

To assess the surface hardness of the Historical Sutlu Minaret Mosque, a Schmidt hammer was used to measure the hardness at 10 different points. The hardness measurements were carried out in accordance with ISRM 1978 [7]. A total of 20 values obtained per sample, as per ASTM D5873-14 [8], and the average value of hardness on the surface was calculated. The hardness measurement results for the walls of the historical mosque are presented in Table 1 for easy reference and analysis.

Table 1. *Schmidt hammer test results*

The mosque	Location	Schmidt hammer (R)
Hacı Mahmut Mosque	Stone	49
	Inner Brick	30.801
	Outer Brick	41.915
	Concrete boarding steps	50
Urla Kamanli Mosque	Stone south 1	30.8
	Stone south 2	31.7
	Stone west 1	39.7
	Stone west 2	38
The Historical Sütlü Minaret Mosque	1	31
	2	36
	3	34
	4	35
	5	51
	6	45
	7	43
	8	45
	9	45
	10	41

2.2. The ultrasonic pulse velocity (UPV)

For Hacı Mahmut Mosque, ultrasonic wave velocity tests were conducted on the materials of the structures using Pundit type equipment. These tests helped to determine the velocity of sound waves passing through the materials, which can provide valuable information about their composition and properties. Furthermore, the stone samples' modulus of elasticity values was determined as per the ASTM (1969) standards [14], which helped to further characterize the mechanical properties of the materials. Table 2 presents the results of the test.

To determine the quality of the brick and stone core samples used in the construction of Urla Kamanli Mosque, an ultrasonic pulse velocity test was conducted. This was accomplished through the

THE ANNALS OF "DUNAREA DE JOS" UNIVERSITY OF GALATI
FASCICLE IX. METALLURGY AND MATERIALS SCIENCE
Nº. 2 - 2023, ISSN 2668-4748; e-ISSN 2668-4756
Article DOI: https://doi.org/10.35219/mms.2023.2.03

use of CNS Farnell Electronic's Pundit type equipment on brick samples (D = 25.6 mm) and stone core (D = 54 mm). The digital unit recorded the time duration for the ultrasonic pulse waves to pass through the sample, and the velocity of the wave was calculated based on the distance between the probes. The results of the ultrasonic pulse velocity test are presented in Table 2 for easy reference and analysis.

Table 2. *The ultrasonic pulse velocity test results of stone and bricks*

The mosque	Sample	Pulse velocity (m/s)	
Hacı Mahmut Mosque	Stone	4030	
	Inner Brick	2170	
	Outer Brick	2304	
	Concrete boarding steps	-	
Urla Kamanli Mosque	Stone south 1	3291	
	Stone south 2	3456	
	Stone west 1	5187	
	Stone west 2	5536	
	Brick	1398	
Al-Omariya mosque		Dry	Saturated
	Brick	1963	2613
The Historical Sütlü Minaret Mosque	Restoration Stone	Vp	Vs
		2773	1642
	Original Stone	3612	2669

To evaluate the quality of the cylindrical brick samples used in the building of Al-Omariya mosque, an ultrasonic pulse velocity (UPV) test was performed. The test was conducted on both dry and saturated (fully vacuum-pressure saturated) cylindrical brick samples (Ø 40 mm x 50 mm) using a pundit pulse apparatus. During the test, a direct pulse was sent from the source electrode through the sample's body, and the pulse was received by the receiver transducer. UPV was calculated by dividing the sample's length by the transmission time of the wave. The test values are presented in Table 2 for easy reference and analysis.

Ultrasound methods were employed to evaluate the quality of the masonry building elements used in The Historical Sütlü

Minaret Mosque. The dynamic elasticity modulus was determined in accordance with ISRM 1978 [7]. Ultrasound velocity measurement tests were conducted at various points within the structure and the results are displayed in Table 2. The propagation velocity of compression (Vp) and shear (Vs) pulses was determined in compliance with ASTM D 2845-05 [9].

2.3. Scanning Electron Microscope (SEM)

To gain a deeper understanding of the stones used in the construction of Urla Kamanli Mosque, microstructural analyses were conducted using the Philips XL 30S-FEG scanning electron microscope (SEM). The samples collected from the west section did not reveal any fossils upon examination. However, upon closer inspection of the stone collected from the south section, fossils ranging from 5-10 µm in outer diameter were investigated.

To conduct a complete analysis of the structural composition of the assessed samples used in the construction of Al-Omariya mosque, an electronic scanner with elevated accuracy, the Hitachi-TM 3000 scanning electron microscope, was employed. This advanced technology allowed for a detailed survey of the samples, providing valuable insights into their composition.

2.4. X-Ray diffraction (XRD)

For Urla Kamanli Mosque, the chemical composition of the stones was concluded via Philips X-Pert X-Ray diffraction (XRD) (PANalytical, Almelo, The Netherlands) and was determined to be calcium carbonate ($CaCO_3$).

For Al-Omariya mosque, the mineral composition of historical samples (mortar and brick) was inspected via the X-Ray Diffraction (XRD) test. Rigaku MiniFlex 600 was used for XRD investigation. To ensure the accuracy and precision of the mineral analysis, a meticulous preparation was carried out, involving the creation of crushed powders from small samples. It is obvious to observe that brick samples are composed principally of quartz (SiO_2) and calcite ($CaCO_3$) as well as of clay minerals and gypsum ($CaSO_4 \cdot 2H_2O$) but in few quantities.

3. Destructive methods

3.1. Uniaxial compression

For Hacı Mahmut Mosque, Uniaxial compression investigations (UAC) were conducted as discussed (TS-699, Ulu say et al. 2001) [5]. The average results are shown in Table 3.

In order to comprehensively analyze the structural integrity of Urla Kamanli Mosque, an array of advanced techniques was employed, including the Uniaxial Compression Test. Which adhered to the guidelines set forth by the International Society for Rock Mechanics (ISRM) (1981) [6], involved subjecting mortar core samples, brick, and stone to rigorous compression forces. The testing was carried out using a state-of-the-art mechanical testing

THE ANNALS OF "DUNAREA DE JOS" UNIVERSITY OF GALATI
FASCICLE IX. METALLURGY AND MATERIALS SCIENCE
Nº. 2 - 2023, ISSN 2668-4748; e-ISSN 2668-4756
Article DOI: https://doi.org/10.35219/mms.2023.2.03

machine that accurately recorded the stroke from the loading head. The stress-strain curves obtained from the uniaxial compression tests were utilized to determine the modulus of elasticity, which corresponded to the tangent modulus at 50% of compressive strength. The resulting averages of the modulus of elasticity and the uniaxial compressive strength of the brick, mortar samples, and stone are presented in Table 3, providing vital insights into the structural properties of the materials used in the construction of the mosque.

Table 3. *Uniaxial compression test results*

The mosque	Sample	Compressive strength (MPa)
Hacı Mahmut Mosque	Stone	58.28
	Inner Brick	13.09
	Outer Brick	18.08
	Concrete boarding steps	7.56
Urla Kamanli Mosque	Stone south 1	64.17
	Stone south 2	65.44
	Stone west 1	127.8
	Stone west 2	105.9
	Brick	11.68
	Mortar Masonry	4.19
	Mortar Brick	8.75
Al-Omariya mosque	Brick	7.02
The Historical Sütlü Minaret Mosque	Original Stone	45.20
	Restoration Stone	13.12
	Mortar	2.20

To succeed a comprehensive understanding of the structural integrity of Al-Omariya mosque, a series of rigorous tests were carried out, including the Uniaxial Compression Test. Three cylindrical samples (Ø 40 mm x 50 mm), dried for two days at 60 °C, were subjected to the test in a dry state condition, in accordance with the standard criteria outlined in [10]. The test was performed using the Instron 4485 press machine, a cutting-edge electronic pressure device, at a loading rate of 0.2 mm/min. The results of the test for the old brick samples are presented in Table 3, providing crucial insights into the materials used in the construction of the mosque. It should be noted, however, that due to the limited dimensions of the mortar samples, not all mechanical tests were feasible.

The Historical Sütlü Minaret Mosque underwent a thorough analysis of its structural integrity, which included the preparation of samples conforming to the guidelines outlined in ISRM 1979 [11]. These samples were carefully crafted with a diameter of 54 mm and a length-to-diameter ratio of 2-2.5, ensuring that they provided an accurate representation of the type materials used in the construction of the mosque. The results of the test, presented in Table 3, provide critical data on the materials' ability to withstand compression forces, offering valuable insights into the mosque's overall structural stability.

3.2. Direct and Indirect tension test

For Hacı Mahmut Mosque, indirect tension tests, also known as Brazilian tests, were conducted on the materials used in the construction in accordance with TS-699, Ulusay *et al.* (2001) standards [15]. The results of these examinations are accessible in Table 4.

The structural integrity of Urla Kamanli Mosque was thoroughly evaluated through the implementation of an Indirect Tension Test on mortar core samples, bricks, and stone - all of which were prepared in strict accordance with the guidelines set forth by the International Society for Rock Mechanics (ISRM) in 1981 [6]. The test results are presented in Table 4 and provide valuable insights into the materials' ability to withstand tension forces, which is critical for ensuring the mosque's long-term stability. The data obtained from the test is crucial for identifying any potential weaknesses in the materials used in the mosque's construction, enabling any necessary repairs or renovations to be carried out with precision and accuracy.

To evaluate the structural integrity of Al-Omariya mosque, direct tensile strength tests were executed on three cylindrical samples (Ø 40 mm x 50 mm) in a dry state condition. Prior to the test, the brick testers were dried for two days using an oven set at 60 °C. The examinations were conducted in accordance with standard criteria outlined in [12], and the samples were subjected to a loading rate of 0.2 mm/min using a programmed electronic pressure device (Instron 4485 press machine). The reaching of the direct tensile strength test for the old brick samples are presented in Table 4, providing valuable data on the materials' ability to withstand tensile forces.

For the Historical Sütlü Minaret Mosque, the indirect tensile strength test was conducted by using the Brazilian test [13]. Table 4 presents the data purchased of the analysed materials.

THE ANNALS OF "DUNAREA DE JOS" UNIVERSITY OF GALATI
FASCICLE IX. METALLURGY AND MATERIALS SCIENCE
N°. 2 - 2023, ISSN 2668-4748; e-ISSN 2668-4756
Article DOI: https://doi.org/10.35219/mms.2023.2.03

Table 4. *Data from direct and indirect tensile strength*

The mosque	Sample	Tensile strength (MPa)
Hacı Mahmut Mosque	Stone	6.09
	Inner Brick	1.43
	Outer Brick	1.43
	Concrete boarding steps	0.75
Urla Kamanli Mosque	Stone south 1	5.72
	Stone south 2	7.41
	Stone west 1	8.49
	Stone west 2	9.88
	Brick	1.867
	Mortar Masonry	0.73
	Mortar Brick	0.95
Al-Omariya mosque	Brick	0.65
The Historical Sütlü Minaret Mosque	Original Stone	4.86
	Restoration Stone	1.82
	Mortar	-

4. Conclusions

In this review paper, the authors aimed to provide a detailed view of the characterization of historical bricks and mortar samples from four significant mosques - Hacı Mahmut Mosque, Urla Kamanli Mosque, Al-Omariya mosque minaret, and the Historical Sütlü Minaret Mosque. The objective was to achieve successful future interventions for the preservation and restoration of these precious cultural and historical landmarks. To accomplish this goal, a mishmash of destructive and non-destructive tests was conducted, including Schmidt rebound hardness test and ultrasonic pulse velocity test to evaluate the hardness and quality of the materials, respectively. In addition, several micro-observation tests, such as XRD and SEM investigations, were performed on the historical samples. Furthermore, the mechanical properties of the samples were explored using uniaxial compression test and direct and indirect tensile strength tests. The meticulous attention to detail in conducting these tests and the use of advanced techniques highlights the importance placed on preserving and protecting these significant historical sites. The findings from this study can serve as valuable resources not only for the restoration of historical mosques and minarets but also for the preservation of other historical monuments dating back to the 15th-16th century. The comprehensive characterization of the materials and determination of their mechanical properties are crucial for identifying any potential weaknesses in the structures and enabling any necessary repairs or renovations to be carried out with precision and accuracy, ensuring the preservation of these precious cultural and historical landmarks for generations to come.

To sum up, this review paper aims to analyse the methods used by the researchers to characterize the materials used in historical mosques and minarets, Additionally, we propose a step-by-step procedure for future studies as follows:

1. Collect the samples without compromising the structural integrity.
2. Conduct non-destructive tests such as macrography and ultrasonic pulse velocity tests etc.
3. Proceed to destructive tests: mechanical tests etc.
4. Analyse the results and engage in a discussion.
5. Establish a correlation between the results and the material properties.

Acknowledgment

We would like to thank the Erasmus+ mobility program for doctoral students with Pitesti University in Romania, for funding the project.

References

[1]. Başaran H., Demir A., Ercan E., Nohutçu H., Hökelekli E., Kozanoğlu C., *Investigation of seismic safety of a masonry minaret using its dynamic characteristics*, Techno-Press, Ltd, Earthquakes and Structures, vol. 10, no. 3, p. 523-538, 2016.

[2]. Hussain A., Akhtar S., *Review of Non-Destructive Tests for Evaluation of Historic Masonry and Concrete Structures*, King Fahd University of Petroleum & Minerals, Arab J Sci Eng., DOI 10.1007/s13369-017-2437-y, 2017.

[3]. Teomete E., Aktaş E., *Structural Analyses and Assessment of Historical Kamanlı Mosque in Izmir, Turkey*, Journal of performance of constructed facilities, ASCE, vol. 24, no. 4, p. 353-364, August 1, 2010.

[4]. Al-Omari A., Khattab S., *Characterization of building materials used in the construction of historical Al-Omariya mosque minaret in Mosul's old city, Iraq*, Journal of Building Engineering, vol. 33, 2020.

[5]. Maras M. M., Özmen A., Sayın E., Ayaz Y., *Seismic Assessment of the Historical Sütlü Minaret Mosque*, Periodica Polytechnica Civil Engineering, 66(2), p. 445-459, 2022.

[6]. ***, *Rock characterization, testing and monitoring: ISRM suggested methods*, International Society for Rock Mechanics (ISRM), 1981.

[7]. ***, *ISRM - Suggested Methods for Determining Sound Velocity*, International Journal of Rock Mechanics and Mining Science and Geomechanical Abstract, 15, p. 53-58, https://doi.org/10.1016/0148-9062(78)91678-9, 1978.

[8]. ***, *ASTM - ASTM D 5873-14 Standard Test Method for Determination of Rock Hardness by Rebound Hammer Method*,

ASTM International, West Conshohocken, PA, USA, https://doi.org/10.1520/D5873-14, 2014.
[9]. ***, *ASTM - D2845-05 Standard Test Method for Laboratory Determination of Pulse Velocities and Ultrasonic Elastic Constants of Rock*, ASTM International, West Conshohocken, PA, USA, https://doi.org/10.1520/D2845-05, 2005.
[10]. ***, *ASTM D2938 - 95 Standard Test Method for unconfined compressive strength of intact rock core specimens*.
[11]. ***, *ISRM - Suggested Methods for Determining the Uniaxial Compressive Strength and Deformability of Rock Materials*, International Journal of Rock Mechanics and Mining Sciences, 15, p. 99-103, 1979.
[12]. ***, *ASTM D2936 - 20 Standard Test Method for Direct Tensile Strength of Intact Rock Core Specimens*.
[13]. Briševac Z., Kujundžić T., Čajić S., *Current Cognition of Rock Tensile Strength Testing by Brazilian Test*, The Mining-Geology Petroleum Engineering Bulletin, 30, p. 101-114, (in Croatian), https://doi.org/10.17794/rgn.2015.2.2, 2015.
[14]. ***, ASTM - D2845-97, 1969, *Standard method for laboratory determination of pulse velocities and ultrasonic elastic constants of rock*, USA, 1996.
[15]. ***, *TS-699 - Natural building stones, Methods of inspection and laboratory testing*, Turkish Standard, Turkey, 1987.

THE ANNALS OF "DUNAREA DE JOS" UNIVERSITY OF GALATI
FASCICLE IX. METALLURGY AND MATERIALS SCIENCE
No. 2 - 2023, ISSN 2668-4748; e-ISSN 2668-4756
Article DOI: https://doi.org/10.35219/mms.2023.2.04

CONSTRUCTION OF THE FH 150 HYDRO-GEOLOGICAL DRILLING FACILITY WITH ADDITIVE MANUFACTURED MARKERS THROUGH 3D PRINTING

Sorin Alexandru FICĂ[1], Andrei DIMITRESCU[2], Claudiu BABIȘ[2]
[1]IPCUP Ploiesti, Romania
[2]Politehnica University from Bucharest, Romania
e-mail: fica_sorin@yahoo.com, andrei_dimitrescu@yahoo.com, claudiubab8@gmail.com

ABSTRACT

The washing head is the most important sub-assembly in a water well drilling installation, and ensures the operation of the installation on the principle of "hydraulic rotary drilling with direct circulation of drilling fluid", whereby, inside the rotating drill rod assembly is injected, through the washhead, drilling fluid from the discharge of the drilling mud pump, which is fed from a pit (pit) dug below ground level.

KEYWORDS: 3D printing, Fused Deposition Modeling, water drilling installation, FH 150

1. Introduction

The purpose of the work is the realization and testing of the FH 150 water well drilling installation, with hydraulic drive, on a monoaxle trailer, in a modern, flexible modular design, for the efficiency, flexibility and reduction of the energy costs of the drilling, being developed 3 innovative modules, namely, the Head Module drilling rig with mechanical drive, the Drilling Head Module with hydraulic drive and the Hydraulic Drive Installation Module, integrated into the monoaxle trailer chassis, which will contain innovative products of the Scientific and Technological Revolution consisting of resistance machine parts and other milestones made through additive manufacturing digitized, namely by 3D FDM printing, Fused Deposition Modeling - Modeling by depositing carbon fiber fusible filament, layer by layer, by hot extrusion, and by digitized subtractive manufacturing, by CNC processing [1].

At this moment, a real industrial, scientific and technological revolution is being discussed worldwide, consisting in the development of Additive Manufacturing AM technologies through the use of 3D printing [2].

In order to modernize the manufacturing program of the FH150 water well drilling rig and to relaunch the research activity, the project proposes the 3D printing of some representative landmarks of the FH150 drilling rig using one of the following technologies:

- FDM (Fused Deposition Modeling) technology, layer by layer in the XoY plane (the thickness of the 3D printed layer is g = 0.1-0.24 mm, the resolution of 3D printing is r = 0.1 mm while the print head advances vertically on the Z axis, layer by layer);
- SLA technology (StereoLitogrAphy – Stereolithography, a laser beam melts and solidifies a special photosensitive resin, layer by layer, in the XoY plane, the thickness of the 3D printed layer g = 0.12-0.24 mm, the resolution of 3D printing is r = 0.05 mm, while the print head advances vertically on the Z axis, layer by layer);
- SLS Technology - Sensitive Laser Sintering, in which a laser beam sweeps and solidifies layer by layer a vat with sinterable powders (including sinterable metal powders).

SLA-StereoLitogrAphy-photosensitive resin bath 3D printing technology, first developed for desktop 3D printers by the American company Formlabs, is used especially for high-resolution 3D printing with special materials, such as HIGH TEMP resin, which it withstands 240 ºC and can be used for 3D printing of moulds for casting rubber articles, or for 3D printing with biomedical resins, or for 3D printing for elastic products [4].

The SLS - Sensitive Laser Sintering printing technology, first developed for desktop 3D printers also by the American company Formlabs, in which a laser beam sweeps and solidifies layer by layer a vat of sinterable powders (including sinterable metal

THE ANNALS OF "DUNAREA DE JOS" UNIVERSITY OF GALATI
FASCICLE IX. METALLURGY AND MATERIALS SCIENCE
Nº. 2 - 2023, ISSN 2668-4748; e-ISSN 2668-4756
Article DOI: https://doi.org/10.35219/mms.2023.2.04

powders), is still immature and the costs of 3D printing with sinterable powders are still very high [5].

It is estimated that the most feasible and with the best price / quality ratio 3D printing technology is FDM (Fused Deposition Modeling) 3D printing technology, first developed for desktop 3D printers by to the American company Maker Bot, which use PLA+, ABS+ or PETG filament. These filaments have a maximum yield strength of Sigma_C = 60 MPa, which is a big disadvantage when 3D printing high-strength parts such as shafts, axes, gears, chain wheels, couplings, etc.

2. Fabrication

For the 3D printing of high-strength parts, the FDM Method X CF 3D printing technology was developed, Modeling by Depositing Fusible Carbon Fiber Filament (CF-Carbon Fiber), filament with the expected yield strength at Sigma_C = 110 MPa, developed technology by the American company Maker Bot Stratasys and also used in the benchmarks of racing cars.

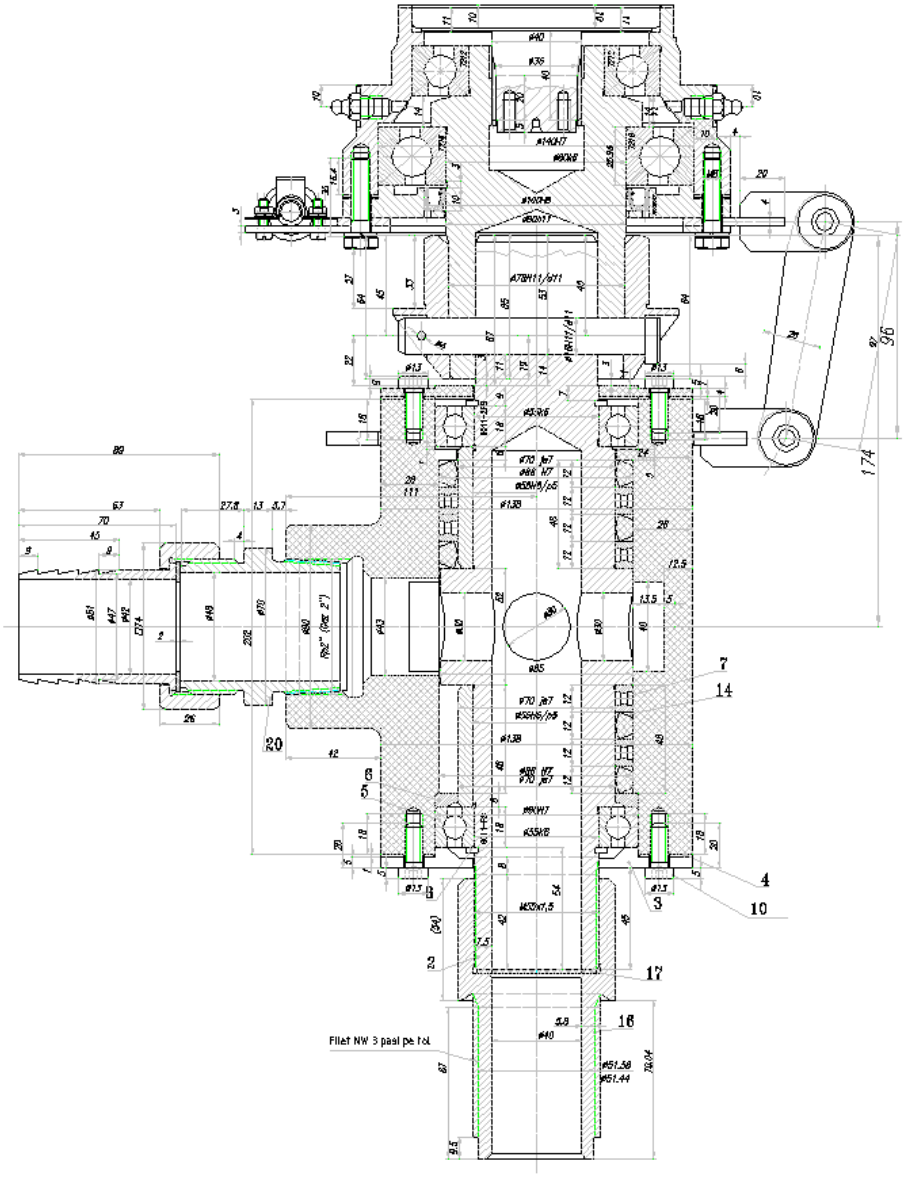

Fig. 1. *The overall drawing of the FA100 washing head, with some landmarks additively manufactured by 3D printing with FDM (Fused Deposition Modeling) technology. The housing of the FA100 washing head has been 3D printed with PETG filament and has therefore been redesigned with thickened walls for increased mechanical strength*

THE ANNALS OF "DUNAREA DE JOS" UNIVERSITY OF GALATI
FASCICLE IX. METALLURGY AND MATERIALS SCIENCE
Nº. 2 - 2023, ISSN 2668-4748; e-ISSN 2668-4756
Article DOI: https://doi.org/10.35219/mms.2023.2.04

The FA100 washing head shown in Figures 1-4 with the casing and the drilling fluid sup-ply fittings, manufactured additively by 3D printing from PETG and ABS+ filament, will be patented with an Industrial Model Patent. The composition table of the "FA100 washing head" assembly drawing is presented in Table 1.

The samples for experimenting with the FA100 washing head, with 3D-printed additively manufactured landmarks, will be made by integrating it into the water well drilling rig with hydraulic drive FA125-FG40, by drilling with it a water well with a depth of H = 20 m and diameter D = 230 mm, by the "rotary-hydraulic drilling method" with direct circulation of drilling fluid, and by maintaining a circulation of abrasive drilling fluid through the washing head FA100 and through the inside of the drill rod assembly, for one week.

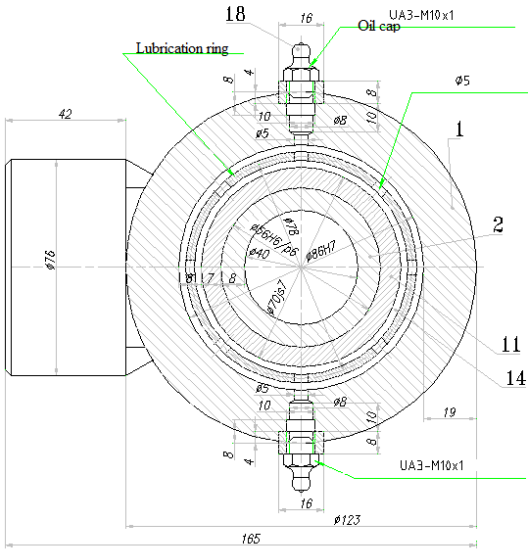

Fig. 2. *Drawing "FA100 washing head", cross section through greasers*

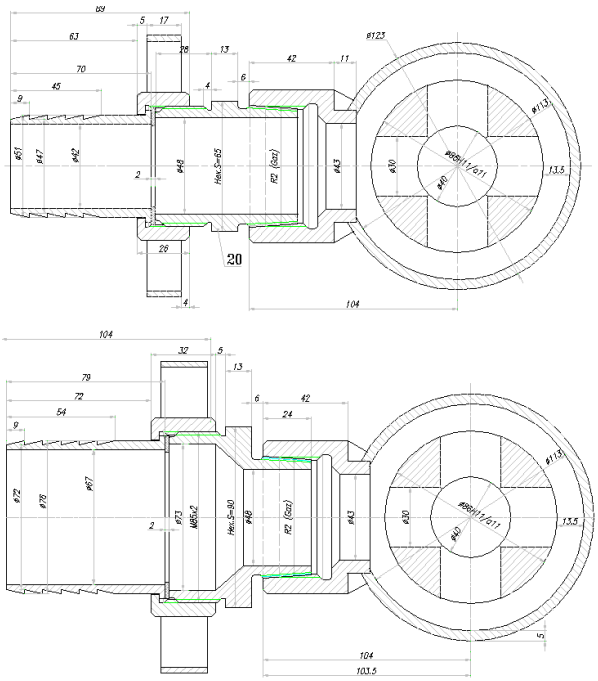

Fig. 3. *Drawing "Washing head FA100", cross section through "R2 Gas Reduction-Hose DN 2in" and through "R2 Gas Reduction-Hose DN 3in*

THE ANNALS OF "DUNAREA DE JOS" UNIVERSITY OF GALATI
FASCICLE IX. METALLURGY AND MATERIALS SCIENCE
No. 2 - 2023, ISSN 2668-4748; e-ISSN 2668-4756
Article DOI: https://doi.org/10.35219/mms.2023.2.04

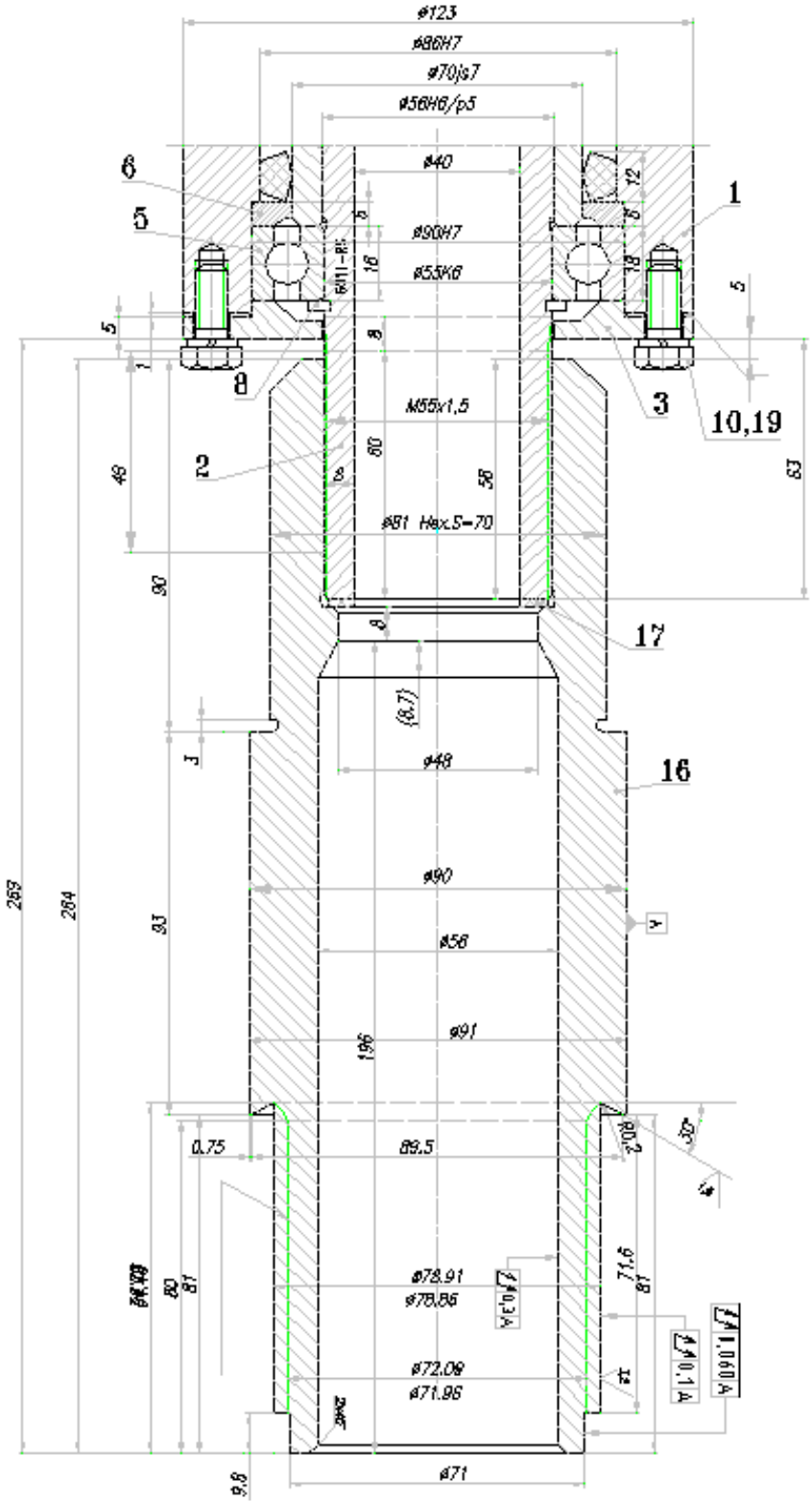

Fig. 4. *Drawing "Washing head FA100", Assembly detail with reduction M55x1.5-Thread HW 3 steps per inch*

THE ANNALS OF "DUNAREA DE JOS" UNIVERSITY OF GALATI
FASCICLE IX. METALLURGY AND MATERIALS SCIENCE
Nº. 2 - 2023, ISSN 2668-4748; e-ISSN 2668-4756
Article DOI: https://doi.org/10.35219/mms.2023.2.04

Tab. 1. *The composition table of the "FA100 washing head" drawing, drawing no. FG40-04.05.00.0*

Poz	Name	Drawing no. or STAS	No.	Materials	Remarks	kg
1	Washing head housing	FG40-04.05.01.0	1	subans.		7.535
2	Washer Head Spindle-M55x1.5	FG40-04.05.02.0	1	42CrMo4	imb. la 310 HB	3.703
3	Lower cover	FG40-04.05.03.0	1	S355J2		0.383
4	Lower gasket	FG40-04.05.04.0	1	Marsit		0.01
5	Radial bearing 8011-RS	SR 3041:1993	2		Ø55xØ90x18	0.21
6	Press bushing	FG40-04.05.06.0	1	CuSn12		0.137
7	Sealing gasket	FG40-04.05.07.0	4	PN70A	Ø70xØ86x12	0.04
8	Shaft elastic ring Ø55	STAS 5848/2-88	2	51Si17A	Ring Ø50,8x2	0.004
9	Top cover	FG40-04.05.09.0	1	S235J2	Gros.4	0.264
10	Screw M8x20	SR ISO 4017:1994	6	gr.8.8		0.01
11	Bush wear	FG40-01.06.11.0	2	42CrMo4	imb.310HB	7.535
12	Screw M6x16	SR ISO 4017:1994	4	gr.8.8		0.004
13	Washer Grower N6	SR 7666-4:94	4	51Si17A		0.01
14	Lubrication ring	FG40-04.05.14.0	4	Cu Sn12	Ø60xØ76x12	0.068
15	Upper gasket	FG40-04.05.15.0	1	Marsit		0.02
16	Reduction M55x1.5-thread HW	FG40-04.05.16.0	1	42CrMo4	imb. la 310 HB	1.051
17	Reduction gasket	FG40-04.05.17.0	1	Marsit	Gros.2	0.01
18	Lubricant UA3	STAS 1116-88	4		M10x1	0.005
19	Washer Grower N8	SR 7666-4:94	6	51Si17A		0.001
20	Adapter Gas R2-Hose DN 2in	FG40-04.05.20.0	1	subans.		1

Conclusions

3D printed FA100 washing head housing prototype, will be additively manufactured by 3D printing and PETG filament on Creality Ender 3 V2 3D printer, Shenzen China. The housing of the FH150 washing head has a value of 1600 lei made of metal materials and classic technologies, having a very low work productivity. In the 3D printed version of PETG and ABS+, it costs only 120 lei, the labour is almost Zero, it is a spectacular leap in work efficiency and productivity.

The theoretical and experimental research that underlies this work is mainly aimed at demonstrating that modern 3D printing technologies can be successfully introduced into the drilling industry.

Thus, the originality of the manufacturing of important milestones for the FH 150 drilling rig was highlighted at the national level. At this moment, we can consider that Romania has taken another important step in the development of Additive Manufacturing AM technologies through the use of 3D printing.

The main challenge after making the landmarks was to demonstrate that they have a strength in operation similar to the original landmarks made of classic materials and technologies.

Acknowledgement

This work was carried out through the Nucleu Program within the National Research Development and Innovation Plan 2022-2027, implemented with the support of MCID, contract no. 42N/2023, project no. PN23140101.

We also thank the external collaborators from the Politehnica University of Bucharest.

References

[1]. Fica Sorin Alexandru, *Realizarea unei instalații inovative de foraj hidrogeologic cu acționare hidraulică a sistemului de manevră si acționare mecanică a capului de foraj de tip FA125*, Programul cercetare NUCLEU, 2017.

[2]. Aamer Nazir, *et al.*, *Multi-material additive manufacturing: A systematic review of design, properties, applications, challenges, and 3D printing of materials and cellular metamaterials*, Elsevier Ltd., vol. 226, 2023.

[3]. Bandyopadhyay A., *Nature-inspired materials and structures using 3D Printing*, Elsevier Ltd., vol. 145, 2021.

[4]. Jiang J., *Machine learning integrated design for additive manufacturing*, Springer, vol. 33, 2022.

[5]. David Rosen, *Design and Manufacturing Implications of Additive Manufacturing*, Journal of Materials Engineering and Performance, vol. 30, 2021.

THE ANNALS OF "DUNAREA DE JOS" UNIVERSITY OF GALATI
FASCICLE IX. METALLURGY AND MATERIALS SCIENCE
N°. 2 - 2023, ISSN 2668-4748; e-ISSN 2668-4756
Article DOI: https://doi.org/10.35219/mms.2023.2.05

ADDITIVE MANUFACTURING THROUGH 3D PRINTING FDM-FUSED DEPOSIT MODELING OF TOP COVER

Sorin Alexandru FICĂ[1], Andrei DIMITRESCU[2], Claudiu BABIȘ[2]
[1]IPCUP Ploiesti, Romania
[2]Politehnica University from Bucharest, Romania
e-mail: fica_sorin@yahoo.com, andrei_dimitrescu@yahoo.com, claudiubab8@gmail.com

ABSTRACT

In this work, it is proposed to make by additive manufacturing through 3D printing with FDM technology FDM (Fused Deposition Modeling - Modeling by Depositing Fusible Filament) some landmarks of the washing head which is common to the light water well drilling rigs FA100, FA125, FH150 and FG40.

A washing head like the FA100 washing head, which has the casing and the drilling fluid supply fittings, 3D printed from PETG and ABS+ filament, has never been made in Romania.

The main advantages of using this manufacturing technology are that by purchasing such equipment, a large number of different landmarks can be made and the final price of the landmark.

KEYWORDS: washing head housing, 3D printing, Fused Deposition Modeling, water drilling installation

1. Introduction

Due to the common use of this flush head on light water well drilling rigs FA100, FA125, FH150 and FG40, its generic name will be "FA100 Flush Head".

The washing head is the most important sub-assembly in a water well drilling installation, and ensures the operation of the installation on the principle of "hydraulic rotary drilling with direct circulation of drilling fluid", whereby, inside the rotating drill rod assembly is injected, through the washhead, drilling fluid from the discharge of the drilling mud pump, which is fed from a pit (pit) dug below ground level.

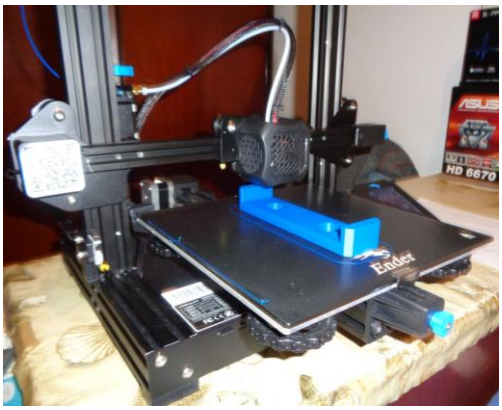

Fig. 1. *Creality Ender 3 V2 3D printer, Shenzhen*

The 3D printed FA100 washing head housing prototype will be additively manufactured through 3D interfacing with PETG filament on the Creality Ender 3 V2 3D printer, Shenzen China. The housing from the FH150 washing head, cost a lot, 1600 lei, before, manufactured by the communist workers from massive welded steel semi-finished products, with very low labour productivity, and with primitive

THE ANNALS OF "DUNAREA DE JOS" UNIVERSITY OF GALATI
FASCICLE IX. METALLURGY AND MATERIALS SCIENCE
No. 2 - 2023, ISSN 2668-4748; e-ISSN 2668-4756
Article DOI: https://doi.org/10.35219/mms.2023.2.05

manufacturing technologies, now in the 3D printed version of PETG and ABS+, it costs only 120 lei, the labour is almost Zero, it is a spectacular leap in work efficiency and productivity.

The FA100 washing head top cap landmark prototype will be manufactured by 3D printing from ABS+ filament on Creality Ender 3 V2 3D printer, Shenzen China [2, 3]. This new variant of realization of the various landmarks offers many advantages compared to the classic realization processes.

The technical characteristics of the printer used are presented in Table 1.

The material used to manufacture the top cover marker is ABS+ with characteristics described in Table 2.

Table 1. *Technical specifications*

Specific technology	FDM (Fused Deposit Modeling - Modeling by Depositing heated fusible filament, layer by layer
Print volume (liters)	12.1
Print dimensions (mm)	220x220x250
Filament diameter (mm)	1.75
Extruders	1, MK10
Print nozzle	Brass, 0.4 mm
Layer thickness (mm)	0.1-0.4
Printing temperature	max. 260
Printing table	Heated, max. 110 °C
Compatible materials	PLA, TPU, ABS, PETG
Display	Color LCD
Command	Rotary knob
Connectivity	USB
External media support	Card SD
Software	Cura (compatible Simplify3D, Repetier Host)
OS compatibility	Windows, Mac, Linux
File format	STL, OBJ, G-code
Feeding	100-265 V 50-60 HZ 270 W
Size (mm)	475x470x620
Net weight (kg)	6.8
Package dimensions (mm)	595x495x165
Package table (kg)	9.6

Table 2. *Characteristics of ABS+*

No. crt.	**Type of filament material for FDM 3D printing**	**Temp. Nozzle 3D Print Head °C**	**Temperature bed printer °C**	**Tensile Strength [MPa]**	**Elongation at Break [%]**	**Flexural Strength [MPa]**	**Flexural Modulus [MPa]**	**Impact Strength [MPa]**
1	ABS+	260	110	40	30	68	2443	42

2. Fabrication

Superior cover landmark, no. drawing FG40-04.05.09.0 was additively manufactured by FDM 3D printing with ABS+ filament according to the drawing in Figure 2.

Figure 3 shows the 3D modeling in the Autodesk Fusion 360 program of the upper cover landmark, which results in the STL format file for "slicing" before its 3D printing.

Figure 4 shows the 3D slicing modeling of the top cover landmark, using the slicing program, Ultimaker Cura 4.13.1

Figures 5 and 6 show the slicing settings of the top cap landmark.

Figure 7 shows the top cap landmark, 3D printed, using ABS+ filament, on the Creality 3D printer, Ender 3 V2.

THE ANNALS OF "DUNAREA DE JOS" UNIVERSITY OF GALATI
FASCICLE IX. METALLURGY AND MATERIALS SCIENCE
No. 2 - 2023, ISSN 2668-4748; e-ISSN 2668-4756
Article DOI: https://doi.org/10.35219/mms.2023.2.05

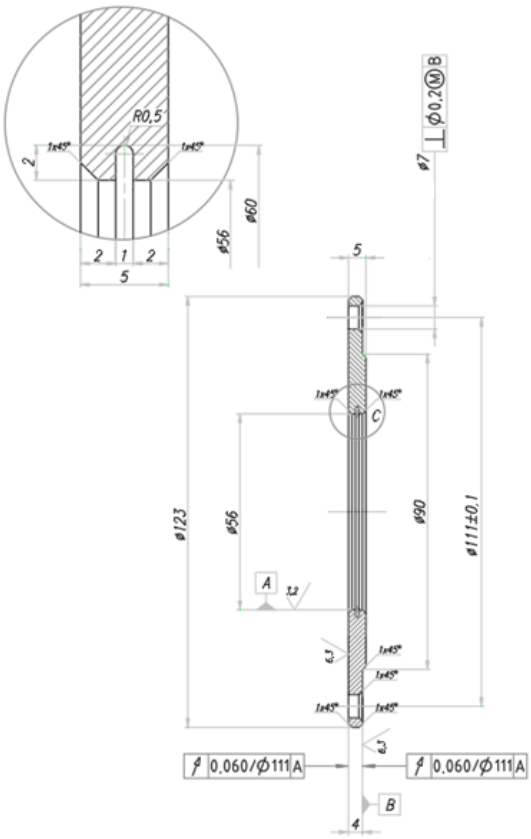

Fig. 2. *Execution drawing - top cover*

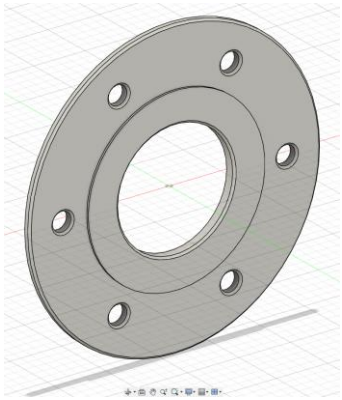

Fig. 3. *3D modeling in Autodesk Fusion 360 of the top cap landmark, resulting in the STL format file for "slicing" before its 3D printing*

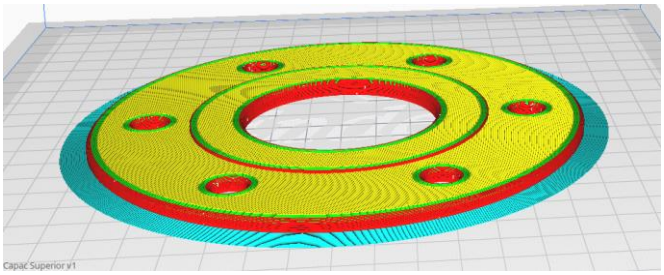

Fig. 4. *3D slicing modeling of the top cap landmark, using the slicing program, Ultimaker Cura 4.11*

THE ANNALS OF "DUNAREA DE JOS" UNIVERSITY OF GALATI
FASCICLE IX. METALLURGY AND MATERIALS SCIENCE
Nº. 2 - 2023, ISSN 2668-4748; e-ISSN 2668-4756
Article DOI: https://doi.org/10.35219/mms.2023.2.05

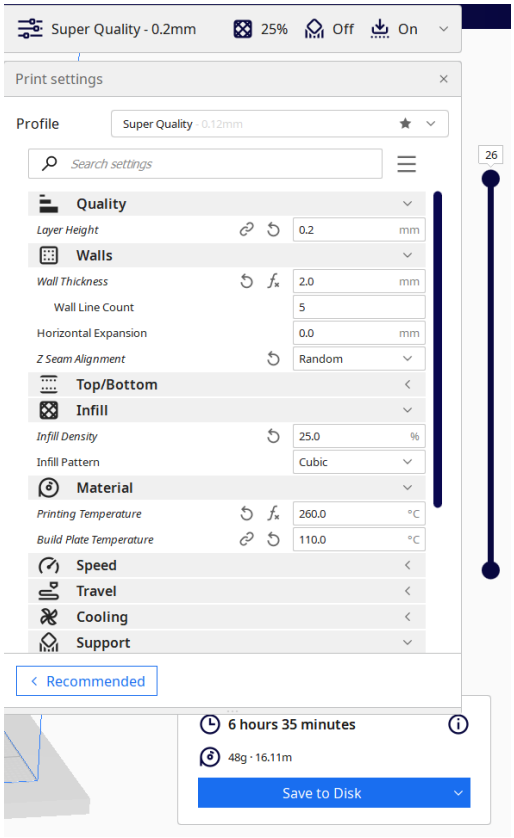

Fig. 5. *Top cap landmark slicing settings*

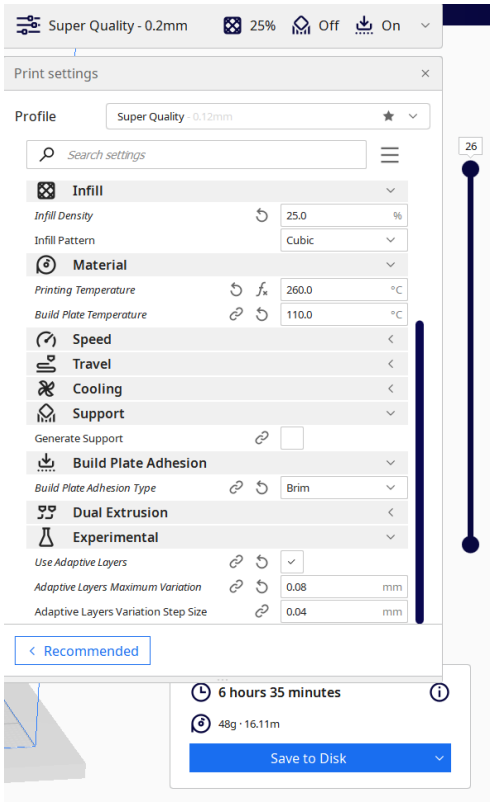

Fig. 6. *Top cap landmark slicing settings*

THE ANNALS OF "DUNAREA DE JOS" UNIVERSITY OF GALATI
FASCICLE IX. METALLURGY AND MATERIALS SCIENCE
N°. 2 - 2023, ISSN 2668-4748; e-ISSN 2668-4756
Article DOI: https://doi.org/10.35219/mms.2023.2.05

Fig. 7. *Top cap landmark 3D printed using ABS+ filament on Creality Ender 3 V2 3D printer*

Conclusions

The realization of landmarks using 3D printing technologies are increasingly widespread in the industry due to the advantages they offer: low energy consumption, very high material utilization efficiency, very high productivity because each printer can be considered a semi-robotic cell and not least the final price that the constructed landmark has.

Also, the built landmark behaved in operation in the same way as the one built from metallic materials using classic technologies.

In the present work, the method of making the "Top cover" landmark using 3D printing technology was experimentally highlighted. Analysing the data, it can be seen that it takes 6 hours and 35 minutes to achieve a higher quality. This time compared to a classic process of obtaining the "Top Cover" landmark, for example by stamping, perforating and embossing, may seem significantly longer, but it must also be taken into account the manufacturing preparation times, which are long in compared to 3D printing technology.

Another factor to consider is the cost of equipment versus machine tools. From this point of view, 3D printing technology is much more advantageous, and the amortization of the investment is done faster than by purchasing machine tools.

We can conclude that the use of 3D printing technologies in the industry is a variant that over time can replace the use of classic technologies.

Acknowledgement

This work was carried out through the Nucleu Program within the National Research Development and Innovation Plan 2022-2027, implemented with the support of MCID, contract no. 42N/2023, project no. PN23140101.

We also thank the external collaborators from the Politehnica University of Bucharest.

References

[1]. Fica Sorin Alexandru, *Realizarea unei instalații inovative de foraj hidrogeologic cu acționare hidraulică a sistemului de manevră si acționare mecanică a capului de foraj de tip FA125*, Programul cercetare NUCLEU, 2017.

[2]. Zukas V., Jonas A. Zukas, *An Introduction in 3D Printing*, First Edition, Design Publishing Inc., 2015.

[3] France A. K., *Make: 3D Printing, the Essential Guide to 3D Printers*, Maker Media, 2020.

[4]. Di Wang, *Recent progress on additive manufacturing of multi-material structures with laser powder bed fusion*, Virtual and Physical Prototyping, vol. 17, 2022.

[5]. Goh G. L., Zhang H., *3D Printing of Multilayered and Multimaterial Electronics: A Review*, John Wiley and Sons Inc, vol. 7, 2021.

THE ANNALS OF "DUNAREA DE JOS" UNIVERSITY OF GALATI
FASCICLE IX. METALLURGY AND MATERIALS SCIENCE
No. 2 - 2023, ISSN 2668-4748; e-ISSN 2668-4756
Article DOI: https://doi.org/10.35219/mms.2023.2.06

ADDITIVE MANUFACTURING THROUGH 3D PRINTING FDM-FUSED DEPOSIT MODELING OF LUBRICATION RING

Sorin Alexandru FICĂ[1], Andrei DIMITRESCU[2], Claudiu BABIȘ[2]
[1]IPCUP Ploiesti, Romania
[2]Politehnica University from Bucharest, Romania
e-mail: fica_sorin@yahoo.com, andrei_dimitrescu@yahoo.com, claudiubab8@gmail.com

ABSTRACT

It presents an element of absolute novelty for industrial scientific research in Romania, the fact that the housing of the washing head and other landmarks of the washing head from the FA100 water well drilling installations. FA125, FH150 and FG40 were made by additive manufacturing by 3D printing with PETG and ABS+ filament.

KEYWORDS: washing head housing, 3D printing, Fused Deposition Modeling, water drilling installation

1. Introduction

The housing of the FG40 washing head costs 1600 lei through classic manufacturing technologies, now in the 3D printed version of PETG and ABS+, it costs only 120 lei, the labour is zero (see Figure 1), thus a major increase in work efficiency and productivity occurs.

Fig. 1. *3D printed FA100 washing head housing at the end of PETG Material, assembled together with the other 3D printed parts of the FA100 washing head*

We are now experiencing some historic moments, for the first time in 70 years of communist and security depravity, Romanian engineers finally have access to their own means of production, represented by 3D printers, now also with high resistance carbon fiber filament, and of machining centres with CNC numerical control, with the status of industrial robots with zero labour.

The manufacture of light water well drilling installations FA75-U, FA100, FA125, FH150 and FG40 represents an absolute degree of novelty for Romania, this research program aligning with the current Re-Industrialization Program of the European Union, generated by the container crisis in China, of the energy, economic and humanitarian crisis and of the crisis of raw materials and materials due to the war in Ukraine, the EU Re-Industrialization program which is carried out in 2 major Development Directions:

A. Additive manufacturing of industrial objects by 3D printing, now also 3D printing by printing high resistance parts with FDM (Fused Deposits Modeling) technology, with Carbon Fiber filament, as in racing cars, with the flow limit Sigma_C = 400

THE ANNALS OF "DUNAREA DE JOS" UNIVERSITY OF GALATI
FASCICLE IX. METALLURGY AND MATERIALS SCIENCE
No. 2 - 2023, ISSN 2668-4748; e-ISSN 2668-4756
Article DOI: https://doi.org/10.35219/mms.2023.2.06

MPa, at unbeatable prices, because 3D Printers have the status of Industrial Robots, with Zero labour; And in Romania a 3D printer has reached extremely low prices, a 3D printer now costs 1500 lei, for example Creality Ender 3 V2. One of the research institutes in the bidding consortium recently acquired a 3D printer with high strength carbon fiber filament, the MakerBot Method X CF Carbon Fiber.

B. The subtractive manufacturing of industrial objects by chipping processing in high-alloy high-strength steels on 3- and 4-axis Numerical Control CNC Machining Centers, and on 2-axis Numerical Control Lathes, at unbeatable prices, because the Centers of CNC processing has the status of industrial robots, with almost zero labour. And in Romania mini CNC machining centers with steel cutting possibilities have arrived at very low prices, for example a CNC 6090 4-axis machining center, with P = 1.5 KW motor, with steel machining possibilities, now costs only 18 000 lei.

These FA75-U, FA100, FA125, FH150 and FG40 lightweight water well rig designs align with the two EU development directions in that high strength water well rig parts can be 3D printed with fiber filament of carbon, like in racing cars [1].

2. Fabrication

Landmark "Oil Ring", No. Drawing FG40-04.05.14.0 was additively manufactured by FDM 3D printing with ABS+ filament according to the drawing in Figure 2.

Figure 3 shows the 3D modeling in the Autodesk Fusion 360 program of the "Lubrication Ring" landmark, which results in the STL format file for "slicing" before its 3D printing.

Figure 4 shows the 3D slicing modeling of the landmark, using the slicing program, Ul-timaker Cura 4.13.1

Figures 5 and 6 show the slicing settings of the top cap landmark.

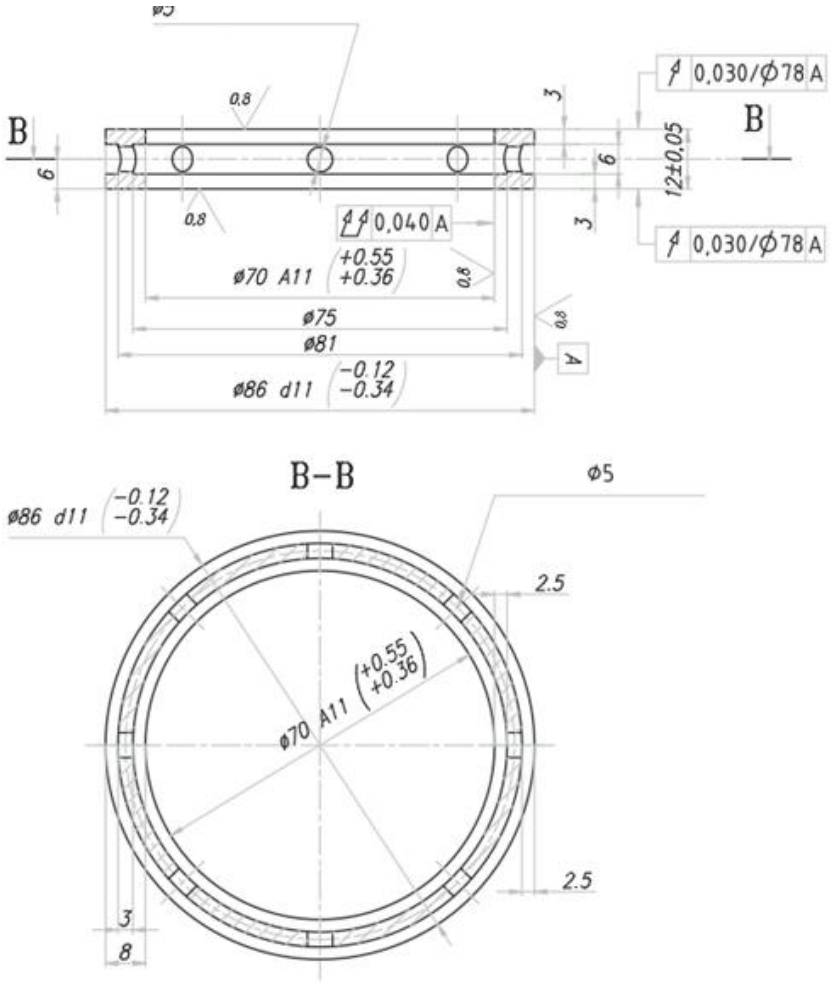

Fig. 2. *Execution drawing – lubrication ring*

THE ANNALS OF "DUNAREA DE JOS" UNIVERSITY OF GALATI
FASCICLE IX. METALLURGY AND MATERIALS SCIENCE
No. 2 - 2023, ISSN 2668-4748; e-ISSN 2668-4756
Article DOI: https://doi.org/10.35219/mms.2023.2.06

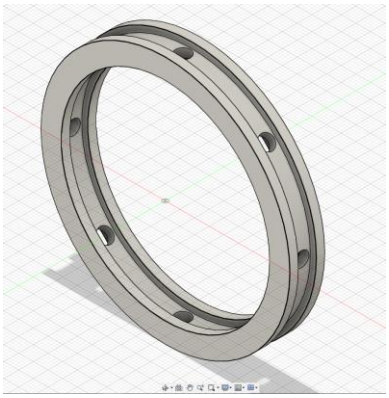

Fig. 3. *3D modeling in the Autodesk Fusion 360 program of the oil ring landmark, resulting in the STL format file for "slicing" before its 3D printing*

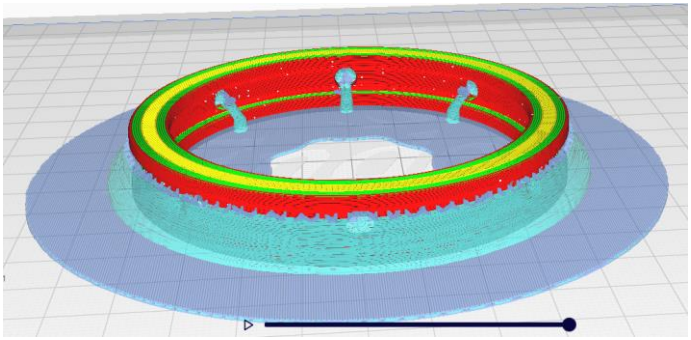

Fig. 4. *3D slicing modeling of the top cap landmark, using the slicing program, Ultimaker Cura 4.11*

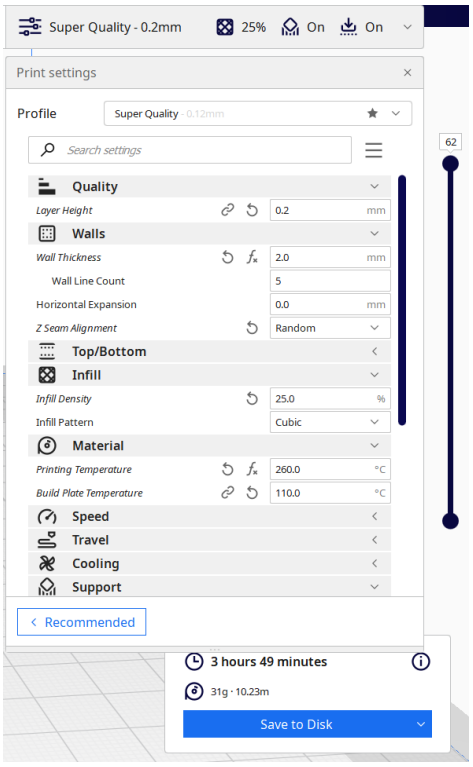

Fig. 5. *The slicing settings of the grease ring reference*

THE ANNALS OF "DUNAREA DE JOS" UNIVERSITY OF GALATI
FASCICLE IX. METALLURGY AND MATERIALS SCIENCE
Nº. 2 - 2023, ISSN 2668-4748; e-ISSN 2668-4756
Article DOI: https://doi.org/10.35219/mms.2023.2.06

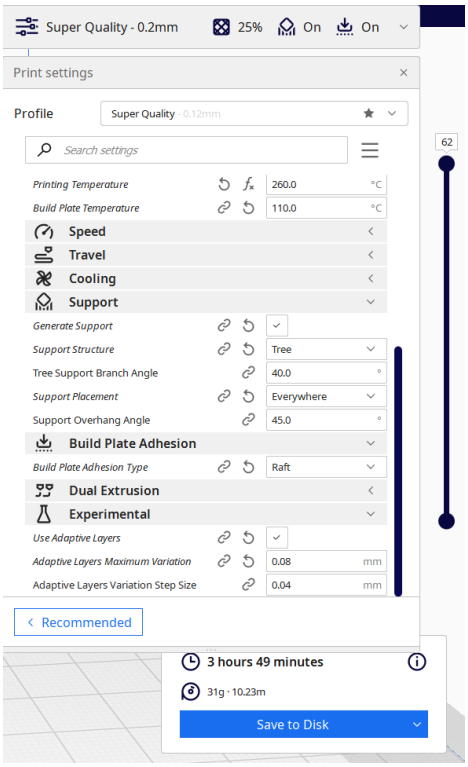

Fig. 6. *The slicing settings of the grease ring reference*

Parameters:

The main slicing settings for the "Grease Ring" feature in Cura 4.13.1 were as follows:

- Layer height = 0.2 mm;
- Wall thickness = 2 mm;
- Z-Seam Alignment = Random;
- Infill density = 25;
- Infill Pattern = Cubic.

Material = ABS+:

- Printing Temperature= 260 ºC;
- Build Plate Temperature= 110 ºC.

Generate Support = Yes:

- Support Structure = Tree;
- Tree Support Branch Angle = 40º;
- Support Placement = Everywhere;
- Support Overhang Angle = 39º;
- Build Plate Adhesion Type = Raft.

Experimental:

- Use Adaptive Layers = Yes;
- Adaptive Layers Maximum Variation = 0.08 mm;
- Adaptive Layers Variation Step Size = 0.04 mm;
- Printing the milestone "Anointing Ring" took 3 hours and 49 minutes. and consumed 31 g of ABS+ filament.

Figure 7 shows the 3D printed landmark, using ABS+ filament, on the Creality 3D printer, Ender 3 V2.

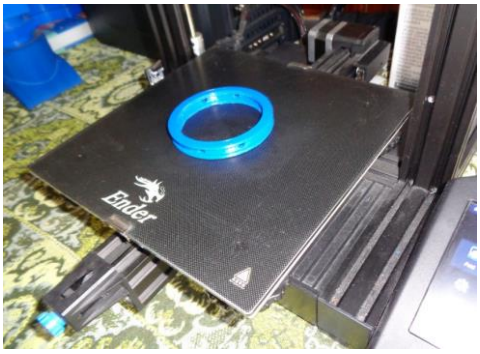

Fig. 7. *Lubrication ring landmark, 3D printed using ABS+ filament, on Creality 3D printer, Ender 3 V2*

THE ANNALS OF "DUNAREA DE JOS" UNIVERSITY OF GALATI
FASCICLE IX. METALLURGY AND MATERIALS SCIENCE
Nº. 2 - 2023, ISSN 2668-4748; e-ISSN 2668-4756
Article DOI: https://doi.org/10.35219/mms.2023.2.06

Conclusions

FA100 washing head housing, 3D printed from PETG material (housing body) and ABS+ (Caps, grease rings, reduction assembly Gas thread Rp2"-M60x2 thread-M60x2 Dutch nut-Dual hose DN50 mm) worked perfectly, without damage and no drilling fluid leaks, during experimental drilling of a water well with the FA125-FG40 drilling rig.

The samples for experimenting with the washing head FA100, with landmarks manufactured additively by 3D printing, were made by integrating it into the water well drilling rig with hydraulic drive FA125-FG40, by drilling with it a water well with a depth of H = 20 m and diameter D = 230 mm, by the "rotary-hydraulic drilling method with direct circulation of drilling fluid, and by maintaining a circulation of abrasive drilling fluid through the washing head FA100 and through the inside of the drill rod gasket, for a week.

The realization of the landmark "Lubrication ring" with the help of 3D printing is an experimental achievement that in 3 hours and 49 minutes can put the drilling rig back into operation by replacing the original part. Practical tests have shown that this landmark fulfils the main function of the part made of classic materials by classic technologies.

The main advantages of 3D printing for the manufacture of the "Lubrication ring" landmark are:

- Possibility of fabrication without the use of bulky machine tools that cannot move to the drilling location. This printer only needs one power source.
- The qualification of the personnel serving the printed matter. With multidisciplinary training a single operator can program the printer and make and replace the part.
- The multitude of landmarks that can be made using the same printer.
- Economy of energy and raw materials.

Acknowledgement

This work was carried out through the Nucleu Program within the National Research Development and Innovation Plan 2022-2027, implemented with the support of MCID, contract no. 42N/2023, project no. PN23140101.

We also thank the external collaborators from the Politehnica University of Bucharest.

References

[1]. Fica Sorin Alexandru, *Realizarea unei instalații inovative de foraj hidrogeologic cu acționare hidraulică a sistemului de manevră si acționare mecanică a capului de foraj de tip FA125*, Programul cercetare NUCLEU, 2017.
[2]. Jiang J., *Machine learning integrated design for additive manufacturing*, Springer, vol. 33, 2022.
[3]. Zukas V., Jonas A. Zukas, *An Introduction in 3D Printing*, First Edition Design Publishing Inc., 2015.
[4]. Aamer Nazir, *et al.*, *Multi-material additive manufacturing: A systematic review of design, properties, applications, challenges, and 3D printing of materials and cellular metamaterials*, Elsevier Ltd., vol. 226, 2023.
[5]. France A. K., *Make: 3D Printing, the Essential Guide to 3D Printers*, Maker Media, 2020.

THE ANNALS OF "DUNAREA DE JOS" UNIVERSITY OF GALATI
FASCICLE IX. METALLURGY AND MATERIALS SCIENCE
Nº. 2 - 2023, ISSN 2668-4748; e-ISSN 2668-4756
Article DOI: https://doi.org/10.35219/mms.2023.2.07

ADDITIVE MANUFACTURING BY 3D PRINTING OF THE LANDMARK GAS REDUCTION R2-M60X2, USING ABS+ FILAMENT

Sorin Alexandru FICĂ[1], Claudiu BABIȘ[2], Andrei DIMITRESCU[2]
[1]ICPE-CA Bucuresti, Romania
[2]Politehnica University from Bucharest, Romania
e-mail: fica_sorin@yahoo.com, claudiubab8@gmail.com, andrei_dimitrescu@yahoo.com

ABSTRACT

This work deals with the additive manufacturing by 3D printing of the Gas Reduction R2-M60x2 landmark which is part of the Gas Reduction R2-Hose DN 2 in subassembly. This sub-assembly is a component part of the washing head of the light water well drilling installations FA 100, FA 125, FH 150 and FG 40. The generic name of the washing head will be FA 100. We use 3D printing technology because, on the one hand, it is technically possible to make the part and on the other hand, for economic reasons. It is approximately ten times cheaper to make the part through 3D printing than through conventional technologies.

KEYWORDS: Gas reduction, 3D printing, Fused Deposition Modeling, water drilling installation

1. Introduction

Due to the common use of the washhead on light water well drilling rigs FA100, FA125, FH150 and FG40, its generic name will be "FA100 Washhead" [1-3].

The aim is to obtain the components of the washing head at water well drilling installations, through 3D printing additive manufacturing, both for technical and economic reasons [4-6]. From an economic point of view, it is approximately ten times cheaper to manufacture the parts of the washing head through 3D printing additive manufacturing than to manufacture them using conventional technologies. This issue represents a spectacular leap in work efficiency and productivity.

This paper deals with the additive manufacturing by 3D printing of the Gas Reduction R2-M60x2, a component part of the washing head of water well drilling installations, generically called FA 100.

The Gas Reduction R2-M2x60 subassembly whose additive manufacturing by 3D printing is to be described is part of the Gas Reducer R2-Hose DN 2 in subassembly, whose component elements are shown in Table 1.

The drawing of the Gas Reduction R2-Hose DN 2 subassembly is presented in Figure 1.

Tabel 1. *Component elements of the R2 Gas Reduction-Hose DN 2 subassembly*

Item	Name	Drawing no. or STAS	Buc.	Material	Remarks	Weight kg
1	Gas ReductionR2-M60x2	FG40-04.05.20.1	1	C45 imb.		0.621
2	Dutch nut M60x2	FG40-04.05.20.2	1	part		0.711
3	Hose pipe DN50 mm	FG40-04.05.20.3	1	S235JR		0.316
4	Flat gasket Ø 58	FG40-04.05.20.4	2	rubber PN70A	Ø58Ø40x2	0.02

THE ANNALS OF "DUNAREA DE JOS" UNIVERSITY OF GALATI
FASCICLE IX. METALLURGY AND MATERIALS SCIENCE
N°. 2 - 2023, ISSN 2668-4748; e-ISSN 2668-4756
Article DOI: https://doi.org/10.35219/mms.2023.2.07

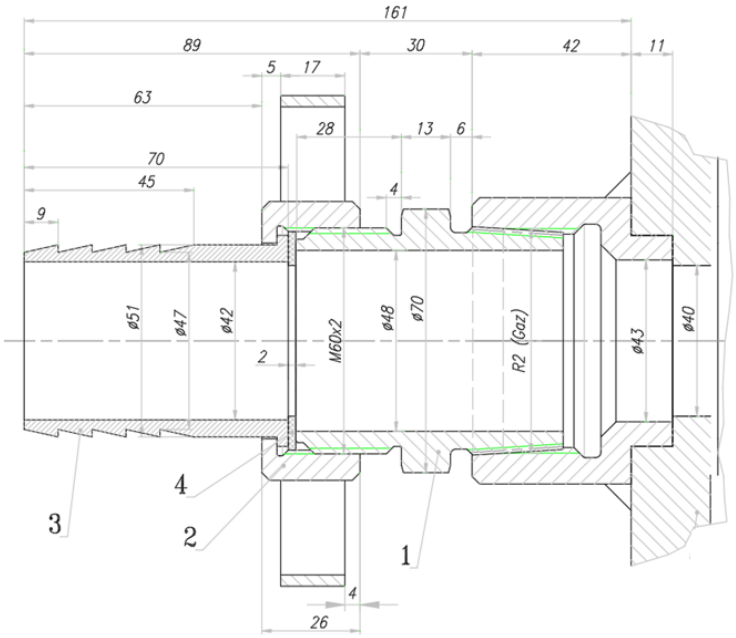

Fig. 1. *Drawing of the R2 Gas Reduction-Hose DN 2 in. subassembly*

2. Fabrication

The 3D-Fused Deposition Modeling printing technology consists in the deposition of fusible material layer by layer in the XoY plane with the thickness of the 3D printed layer between 0.12-0.24 mm, the printing resolution being r = 0.1 mm, while the head printhead advances vertically on the Z axis.

For ABS+ type 3D printing filaments, Shenzen China Creality Ender 3 V2 type 3D printer will be used. Figure 2 shows the printer we used to manufacture the Gas Reduction R2-M2x60 benchmark.

Some technical specifications of the 3D printer used are presented below.

- 3D printing technology: FDM- Fused Deposition Modeling;
- Extruder type: Bowden;
- Minimum number of extruders: 1;
- Maximum number of extruders: 1;
- Compatible filament: PLA; PETG; TPU ABS+; PLA+;
- Print support material: Glass;
- Frame type: open;
- Maximum layer height: 0.4 mm;
- Minimum layer height: 0.1 mm;
- Fill [%]: 0%-100%- Interior filling model: Fast honeycomb Full honeycomb Wiggle Triangular Grid – Rectilinear;
- Outer filling model: Rectilinear Concentric;
- Maximum temperature [℃]: 260;
- Maximum print speed [mm³/s]: 180;
- Minimum print speed [mm³/s]: 10;
- Maximum layer resolution [mm]: 0.4;
- Minimum layer resolution [mm]: 0.1;
- Software included: Cura;
- Filament diameter [mm]: 1.75;
- Nozzle diameter [mm]: 0.4 mm;
- Length [mm]: 475 mm;
- Width [mm]: 470 mm;
- Height [mm]: 620.

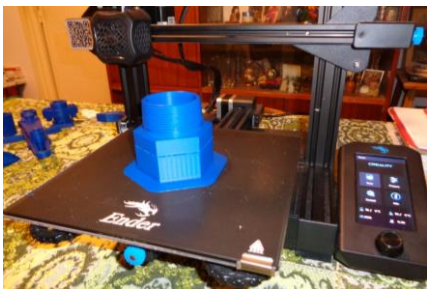

Fig. 2. *3D Printer Creality Ender 3 V2 used in the manufacture of the R2 Gas Reducer-Hose DN 2 in*

THE ANNALS OF "DUNAREA DE JOS" UNIVERSITY OF GALATI
FASCICLE IX. METALLURGY AND MATERIALS SCIENCE
No. 2 - 2023, ISSN 2668-4748; e-ISSN 2668-4756
Article DOI: https://doi.org/10.35219/mms.2023.2.07

It starts from the sketch of the longitudinal section of the FA100 washing head housing, necessary for the generation of Solid 3D by revolutionizing the 3D model, within the Autodesk Fusion 360 program [4]. Figure 2 shows the 3D modeling in the Autodesk Fusion 360 program of the landmark "FA100 washing head housing", which results in the STL format file for "slicing" before its 3D printing.

The R2-M60x2 Gas Reduction landmark is additively manufactured by 3D FDM printing with ABS+ filament whose characteristics are presented in Table 2.

The R2-M60x2 Gas Reduction landmark made by 3D printing must be in accordance with the execution drawing in Figure 3.

Figure 4 shows the 3D modeling in the Autodesk Fusion 360 program of the "Gas Reduction R2-M60x2" landmark, which results in the STL format file for "slicing" before its 3D printing.

Table 2. *Features ABS+ filament*

No	Type of filament material for FDM 3D printing	Temp. Nozzle 3D Print Head ºC	Temperature bed printer ºC	Tensile Strength [MPa]	Elongation at Break [%]	Flexural Strength [MPa]	Flexural Modulus [MPa]	Strength [MPa]
1	ABS+	260	110	40	30	68	2443	42

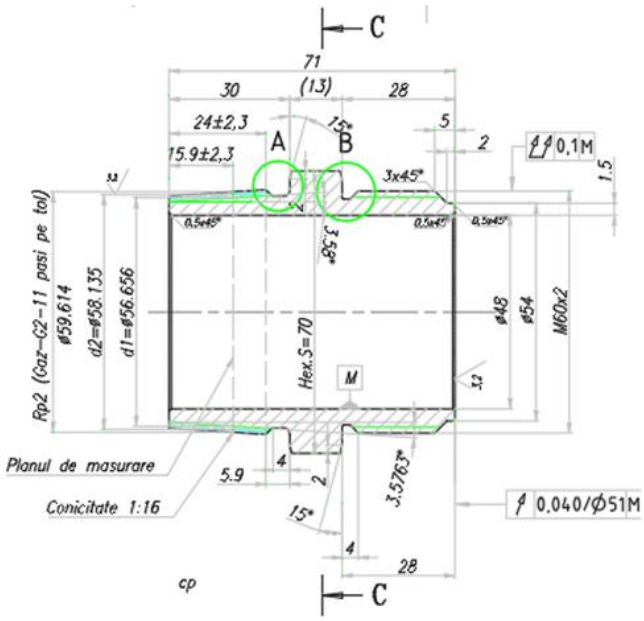

Fig. 3. *Execution drawing for the R2-M60x Gas Reduction benchmark 2*

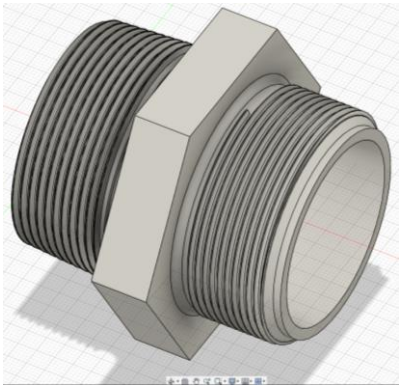

Fig. 4. *3D Modeling in the Autodesk Fusion 360 program of the landmark "Gas Reduction R2-M60x2*

THE ANNALS OF "DUNAREA DE JOS" UNIVERSITY OF GALATI
FASCICLE IX. METALLURGY AND MATERIALS SCIENCE
Nº. 2 - 2023, ISSN 2668-4748; e-ISSN 2668-4756
Article DOI: https://doi.org/10.35219/mms.2023.2.07

Figure 5 shows the slicing of the Gas Reducer R2-M60x2 benchmark, with the help of the slicing program, Ultimaker Cura 4.13.1.

Figure 6 shows some of the settings for slicing the Gas Reduction R2-M60x2 benchmark.

Other settings made for slicing the Gas Reduction R2-M60x2 benchmark are shown in Figure 7.

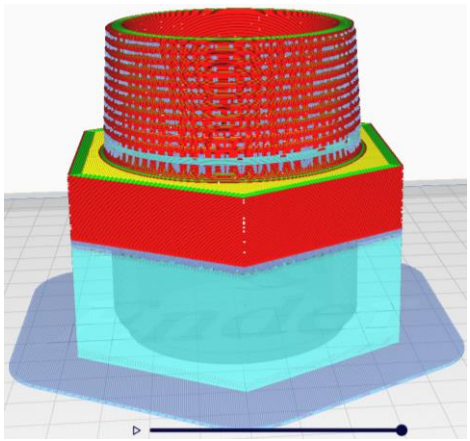

Fig. 5. *Slicing the landmark "Gas reduction R2-M60x2, using the Ultimaker Cura 4.13.1 program*

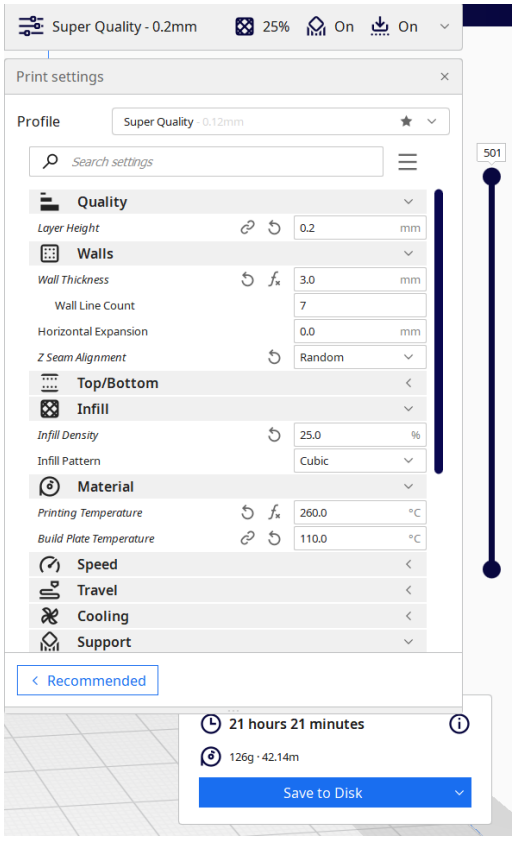

Fig. 6. *The first part of the settings for slicing the "Gas Reduction R2-M60x2" landmark, using the Ultimaker Cura 4.13.1 program*

THE ANNALS OF "DUNAREA DE JOS" UNIVERSITY OF GALATI
FASCICLE IX. METALLURGY AND MATERIALS SCIENCE
Nº. 2 - 2023, ISSN 2668-4748; e-ISSN 2668-4756
Article DOI: https://doi.org/10.35219/mms.2023.2.07

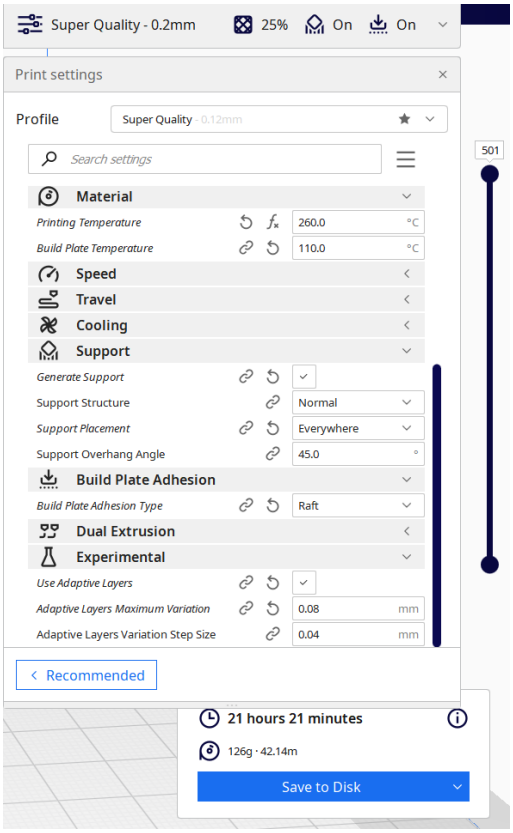

Fig. 7. *The second part of the settings for slicing the landmark "Gas reduction R2-M60x2, using the Ultimaker Cura 4.13.1 program*

The main slicing settings for the R2-M60x2 Gas Reduction benchmark, in the Cura 4.13.1 program, were as follows: Layer height = 0.2 mm; Wall thickness = 4 mm; Z-Seam Alignment = Random; Infill density = 25; Infill Pattern = Cubic; Material = ABS+; Printing Temperature = 260 ºC; Build Plate Temperature = 110 ºC; Generate Support = Yes; Support Structure = Tree; Tree Support Branch Angle = 40º; Support Placement = Everywhere; Support Overhang Angle = 39º; Build Plate Adhesion Type = Raft; Use Adaptive Layers = Yes; Adaptive Layers Maximum Variation = 0.08 mm; Adaptive Layers Variation Step Size = 0.04 mm.

The benchmark "Gas Reduction R2-M60x2" took 21 hours and 21 minutes to print. and consumed 126 g of ABS+ filament. The Slice command is given.

The Gas Reduction landmark R2-M60x2 manufactured by 3D additive printing on the Creality Ender 3 V2 3D printer, using ABS+ filament is presented in Figure 8.

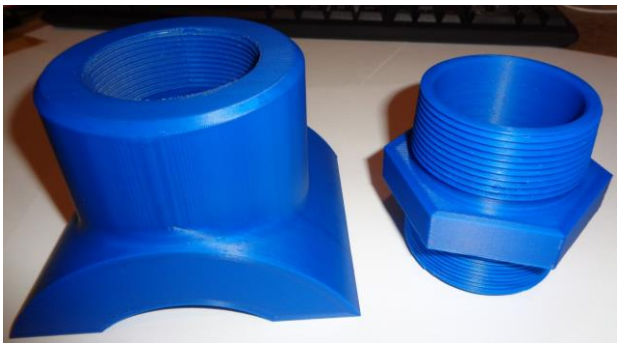

Fig. 8. *The landmark Gas Reduction R2-M60x2 manufactured by additive 3D printing on the Creality Ender 3 V2 3D printer*

THE ANNALS OF "DUNAREA DE JOS" UNIVERSITY OF GALATI
FASCICLE IX. METALLURGY AND MATERIALS SCIENCE
N°. 2 - 2023, ISSN 2668-4748; e-ISSN 2668-4756
Article DOI: https://doi.org/10.35219/mms.2023.2.07

Conclusions

The manufacture of the benchmark Gas Reduction R2-M60x2, through 3D printing, represented the optimal solution from a technical and economic point of view. In the conventional manufacturing version, a high manufacturing cost results and the labour productivity was low. In the 3D printed version made of ABS+ filament, the part costs approximately 10 times less, the labour being almost zero. This issue represents a spectacular leap in work efficiency and productivity.

This landmark is an integral part of the washing head from light water well drilling installations, type FA 100, FA 125, FH 150 and FG 40. The additive manufacturing by 3D printing of this landmark aims to reduce the manufacturing cost of light drilling installations water wells thus falling into the category of green projects and projects for the realization of industrial parts through additive methods.

The partial realization through additive manufacturing through 3D printing of some land-marks of light water well drilling installations has several advantages. On the one hand, from an economic point of view, the reduction of the manufacturing cost is obtained, and on the other hand, a modern, fast and relatively easy to implement technical solution is used.

Another objective pursued by the manufacture of light installations for drilling water wells at low costs and using modern technical solutions such as additive manufacturing through 3D printing, is the relaunch of irrigation in Romania. This is a requirement of the European commissioners in the National Recovery and Resilience Plan of Romania PNRR. The proposed solution is to make water wells with drilling installations, or a water well with a depth of 80 meters, on two hectares of land agricultural.

Taking into account the fact that Romania's agricultural area is 13.8 million hectares, and that there is the ability to irrigate 2 hectares of agricultural land, by drilling a water well with a depth of H = 80 m, it is expected that in the coming years the need to drill approximately 6 mil-lion water wells with H = 80 m. For this, it is expected to carry out in series production a number of 60 thousand light FA100 water well drilling installations, for hydrogeological drilling in favourable plain areas, without particular geological problems, for example in the Mostiștea aquifer, with a depth of H = 80 m, below Bucharest-Ilfov and neighbouring counties, and the realization in series production of a number of 10 thousand hydrogeological drilling rigs FH150, modular, with hydraulic drive, on monoaxle trailer, for drilling water wells in difficult geological areas, hilly with hard geological layers (limestone, sandstone, shale, conglomerate, gravel and boulder, etc.).

In this sense, the approach of manufacturing the components of light water well drilling installations, at the level of Romania, through additive methods such as 3D printing, is a perfectly justified technical-economic solution.

Acknowledgement

This work was carried out through the Nucleu Program within the National Research Development and Innovation Plan 2022-2027, implemented with the support of MCID, contract no. 42N/2023, project no. PN23140101.

We also thank the external collaborators from the Politehnica University of Bucharest.

References

[1]. Fica Sorin Alexandru, *Realizarea unei instalații inovative de foraj hidrogeologic cu acționare hidraulică a sistemului de manevră si acționare mecanică a capului de foraj de tip FA125*, Programul cercetare NUCLEU, 2017.

[2]. Fica Sorin Alexandru, *Additive manufacturing through 3D printing FDM-Fused Deposit Modeling of press bush*, Editura Academica Brâncuși, Târgu Jiu, ISSN 1844-640X, Fiability and Durability, no 1, 2023.

[3]. Fica Sorin Alexandru, *Washing Head Housing, 3D printing from FA 100 drilling installation, using PETG fillament*, Editura Academica Brâncuși, Târgu Jiu, ISSN 1844-640X, Fiability and Durability, no 1, 2023.

[4]. Zukas V., Jonas A. Zukas, *An introduction in 3D printing*, First Edition, Design Publishing Inc., 2015.

[5]. France A. K., *Make: 3D Printing, the Essential Guide to 3D Printers*, Maker Media, 2020.

[6]. Wild J., *Fusion 360 Step by Step*, Landau, Germany, 2021.

THE ANNALS OF "DUNAREA DE JOS" UNIVERSITY OF GALATI
FASCICLE IX. METALLURGY AND MATERIALS SCIENCE
N°. 2 - 2023, ISSN 2668-4748; e-ISSN 2668-4756
Article DOI: https://doi.org/10.35219/mms.2023.2.08

ADDITIVE MANUFACTURING THROUGH 3D PRINTING OF THE LANDMARK NUT M60X2, USING ABS+ FILAMENT

Sorin Alexandru FICĂ[1], Claudiu BABIȘ[2], Andrei DIMITRESCU[2]
[1]ICPE-CA Bucuresti, Romania
[2]Politehnica University from Bucharest, Romania
e-mail: fica_sorin@yahoo.com, claudiubab8@gmail.com, andrei_dimitrescu@yahoo.com

ABSTRACT

This paper deals with the additive manufacturing by 3D printing of the Dutch Nut-M60x2 landmark which is part of the subassembly Gas Reducer R2-Hose DN 2 in. This subassembly is a component part of the washing head of the light water well drilling installations FA 100, FA 125, FH 150 and FG 40. The generic name of the washing head will be FA 100.We use 3D printing technology because, on the one hand, it is technically possible to make the part and on the other hand, for economic reasons. It is approximately ten times cheaper to make the part through 3D printing than through conventional technologies

KEYWORDS: Dutch nut, 3D printing, Fused Deposition Modeling, water drilling installation

1. Introduction

Due to the common use of the washhead on light water well drilling rigs FA100, FA125, FH150 and FG40, its generic name will be "FA100 Washhead" [1-3].

The aim is to obtain the components of the washing head at water well drilling installations, through 3D printing additive manufacturing, both for technical and economic reasons [4-6]. From an economic point of view, it is approximately ten times cheaper to manufacture the parts of the washing head through 3D printing additive manufacturing than to manufacture them using conventional technologies. This issue represents a spectacular leap in work efficiency and productivity.

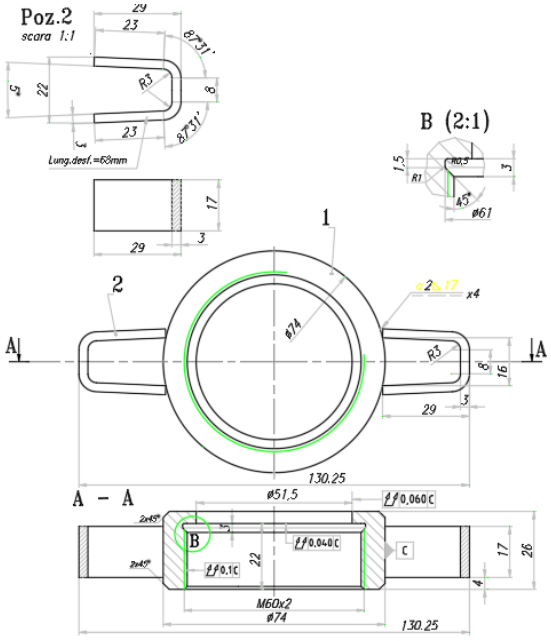

Fig. 1. *Execution drawing Dutch Nut M60x2*

THE ANNALS OF "DUNAREA DE JOS" UNIVERSITY OF GALATI
FASCICLE IX. METALLURGY AND MATERIALS SCIENCE
Nº. 2 - 2023, ISSN 2668-4748; e-ISSN 2668-4756
Article DOI: https://doi.org/10.35219/mms.2023.2.08

This paper deals with the additive manufacturing by 3D printing of the Dutch Nut-M60x2, a component part of the washing head of water well drilling installations, generically called FA 100.

The landmark M60x2 Dutch Nut, whose additive manufacturing through 3D printing is to be described, is part of the Gas Reducer R2-Pipe DN 2 subassembly.

The M60x2 Dutch Nut landmark was fabricated by FDM 3D printing with ABS+ filament according to the drawing in Figure 1.

2. Fabrication

Figure 2 shows the 3D modeling before slicing of the Dutch Nut M60x2, using the slicing program, Ultimaker Cura 4.13.1.

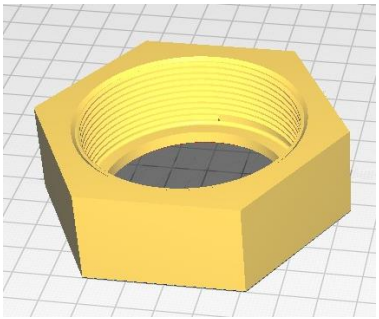

Fig. 2. *3D Modeling of the M60x2 Dutch Nut landmark before slicing, using the slicing program, Ultimaker Cura 4.13.1*

Figure 3 shows the 3D modeling after slicing of the M60x2 M60x2 Flat nut, using the slicing program, Ultimaker Cura 4.13.1.

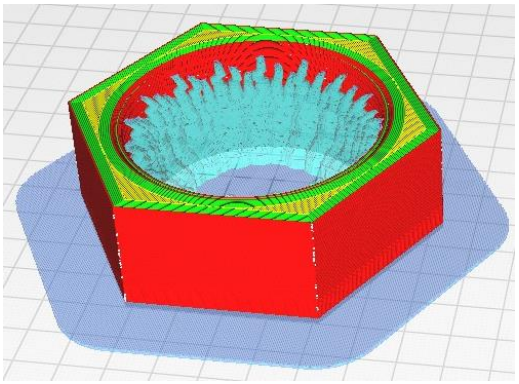

Fig. 3. *3D modeling after slicing of the M60x2 Dutch Nut landmark, using the slicing program, Ultimaker Cura 4.13.1*

Figure 4 shows some of the settings for slicing the landmark Nut M60x2.

Other settings made for slicing the M60x2 Dutch Nut Reduction benchmark are shown in Figure 5.

The third part of the settings made for slicing the mark Reduction Dutch Nut M60x2 are presented in Figure 6.

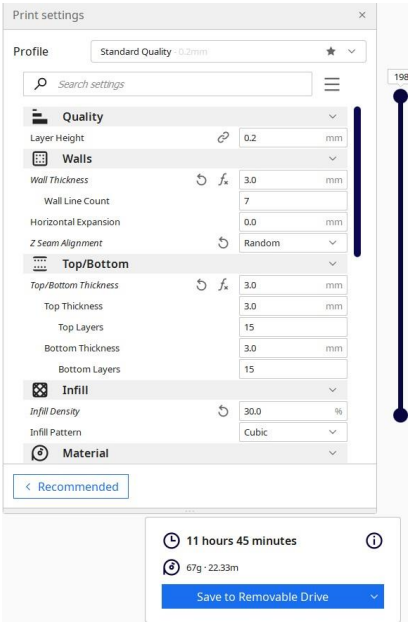

Fig. 4. *The first part of the settings for slicing the Dutch Nut landmark, using the Ultimaker Cura 4.13.1 program*

THE ANNALS OF "DUNAREA DE JOS" UNIVERSITY OF GALATI
FASCICLE IX. METALLURGY AND MATERIALS SCIENCE
Nº. 2 - 2023, ISSN 2668-4748; e-ISSN 2668-4756
Article DOI: https://doi.org/10.35219/mms.2023.2.08

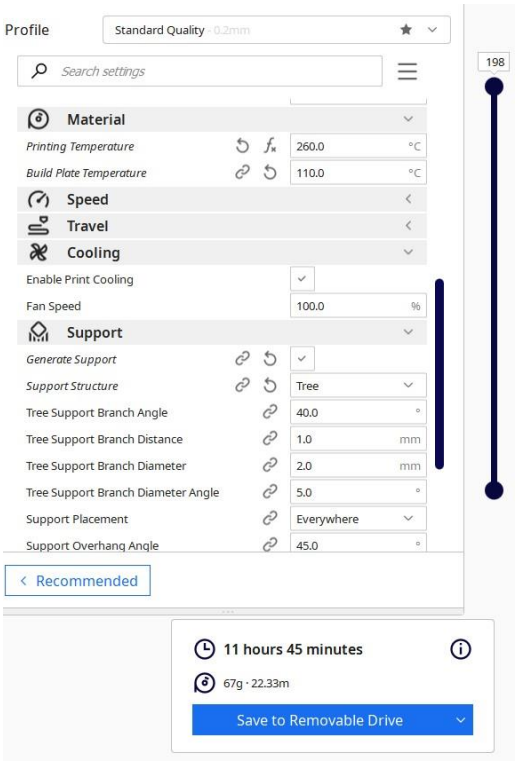

Fig. 5. *The second part of the settings for slicing the Dutch Nut landmark, using Ultimaker Cura 4.13.1*

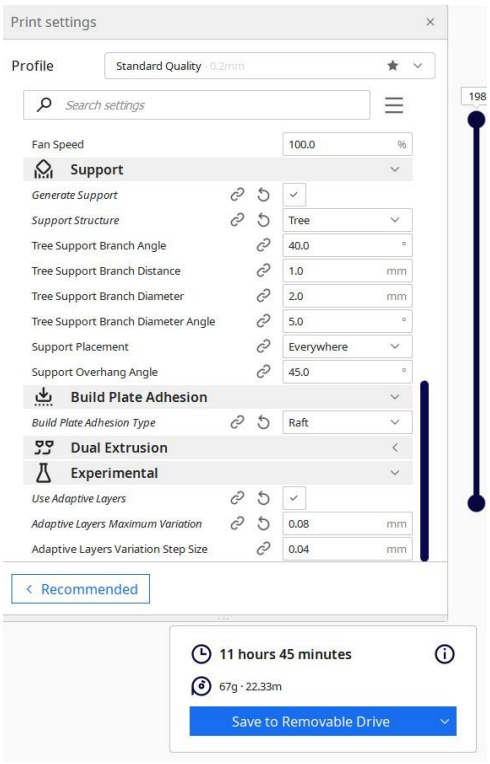

Fig. 6. *The third part of the settings for slicing the Dutch Nut landmark, using Ultimaker Cura 4.13.1*

The main slicing settings for the "Dutch Nut M60x2" feature, in Cura 4.13.1, were as follows: Layer heigh t= 0.2 mm; Wall thickness = 3 mm; Z-Seam Alignment = Random; Infill density = 30; Infill

THE ANNALS OF "DUNAREA DE JOS" UNIVERSITY OF GALATI
FASCICLE IX. METALLURGY AND MATERIALS SCIENCE
No. 2 - 2023, ISSN 2668-4748; e-ISSN 2668-4756
Article DOI: https://doi.org/10.35219/mms.2023.2.08

Pattern = Cubic; Material = ABS+; Printing Temperature = 260 ºC; Build Plate Temperature = 110 ºC; Generate Support = Yes; Support Structure = Tree; Tree Support Branch Angle = 40º; Support Placement = Everywhere; Support Overhang Angle = 39º; Build Plate Adhesion Type = Raft; Experimental; Use Adaptive Layers = Yes; Adaptive Layers Maximum Variation = 0.08 mm; Adaptive Layers Variation Step Size = 0.04 mm.

Dutch Nut M60x2 benchmark took 11 hours and 45 minutes to print. and consumed 67 g of ABS+ filament. The Slice command is given.

Figure 7 shows the Dutch Nut M60x2, 3D printed using ABS+ filament on the Creality 3D printer, Ender 3 V2.

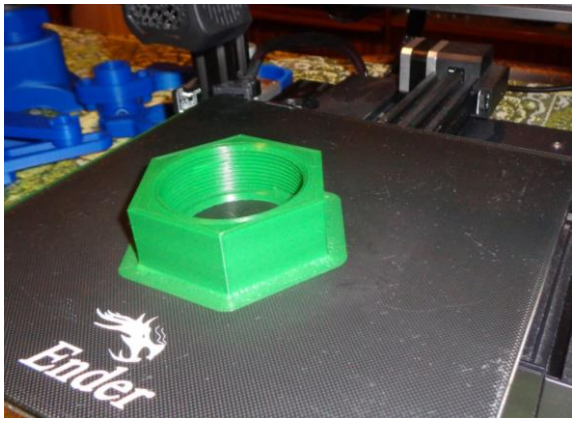

Fig. 7. *Landmark M60x2 Dutch Nut manufactured by additive 3D printing on the Creality Ender 3 V2 3D printer*

Conclusions

The manufacture of the Dutch nut-M60x2 landmark, through 3D printing, represented the optimal solution from a technical and economic point of view. In the conventional manufacturing version, a high manufacturing cost results and the labour productivity was low. In the 3D printed version made of ABS+ filament, the part costs approximately 10 times less, the labour being almost zero. This issue represents a spectacular leap in work efficiency and productivity.

This landmark is an integral part of the washing head from light water well drilling installations, type FA 100, FA 125, FH 150 and FG 40. The additive manufacturing by 3D printing of this landmark aims to reduce the manufacturing cost of light drilling installations water wells thus falling into the category of green projects and projects for the realization of industrial parts through additive methods.

The partial realization through additive manufacturing through 3D printing of some landmarks of light water well drilling installations has several advantages. On the one hand, from an economic point of view, the reduction of the manufacturing cost is obtained, and on the other hand, a modern, fast and relatively easy to implement technical solution is used.

Another objective pursued by the manufacture of light installations for drilling water wells at low costs and using modern technical solutions such as additive manufacturing through 3D printing, is the relaunch of irrigation in Romania. This is a requirement of the European commissioners in the National Recovery and Resilience Plan of Romania PNRR. The proposed solution is to make water wells with drilling installations, or a water well with a depth of 80 meters, on two hectares of land agricultural.

Romania's National Strategy on Climate Change requires the adoption of measures to mitigate the effects of global warming and the prolonged drought caused by global warming, and therefore the declaration of water as a strategic national reserve in Romania, and real-time monitoring of strategic water reserves is aimed at contained in the underground aquifers of Romania.

The water in the underground aquifer layers (which are porous geological layers made of gravel and sand) accumulates in the aquifer for thousands of years and the water in the aquifer has a very low circulation speed of 1 m/year. Of the world's fresh water resources, 68.3% are ice caps and glaciers, 31.4% are water from underground aquifers and only 0.3% are fresh surface water, so the most important fresh water resources that can be efficiently exploited they are those from the underground aquifers, which are proposed to be monitored and managed efficiently, intelligently and in real time through the topic at hand. Even if there are dry periods, the underground aquifer is replenished with water and the water is stored in the aquifer, without evaporating,

during rainy periods. So now, there is sufficient water in the aquifers from the depth H = 80 m in the underground of Romania.

At the moment, water is a strategic resource in the European Union. In this context, knowing the disposition of the aquifers on the surface of Romania and at depth, it is proposed to create, by drilling with FH100 type installations, a network of intelligent IOT-Internet of Things type wells, for monitoring the underground water level at the depth H=80m, connected in real time via Arduino microcontrollers with WiFi transmission to the Internet Router, which will indicate in real time on the internet page of the water well the depth at which the underground water is located, for the respective area.

In this sense, the approach of manufacturing the components of light water well drilling installations, at the level of Romania, through additive methods such as 3D printing, is a perfectly justified technical-economic solution.

Acknowledgement

This work was carried out through the Nucleu Program within the National Research Development and Innovation Plan 2022-2027, implemented with the support of MCID, contract no. 42N/2023, project no. PN23140101.

We also thank the external collaborators from the Politehnica University of Bucharest.

References

[1]. Fica Sorin Alexandru, *Realizarea unei instalații inovative de foraj hidrogeologic cu acționare hidraulică a sistemului de manevră si acționare mecanică a capului de foraj de tip FA125*, Programul cercetare NUCLEU, 2017.

[2]. Fica Sorin Alexandru, *Additive manufacturing through 3D printing FDM-Fused Deposit Modeling of press bush*, Editura Academica Brâncuși, Târgu Jiu, ISSN 1844-640X, Fiability and Durability, no. 1, 2023.

[3]. Fica Sorin Alexandru, *Washing Head Housing, 3D printing from FA 100 drilling installation, using PETG fillament*, Editura Academica Brâncuși, Târgu Jiu, ISSN 1844-640X, Fiability and Durability, no. 1, 2023.

[4]. Zukas V., Jonas A. Zukas, *An Introduction in 3D Printing*, First Edition, Design Publishing Inc., 2015.

[5]. France A. K., *Make: 3D Printing, the Essential Guide to 3D Printers*, Maker Media, 2020.

[6]. Wild J., *Fusion 360 Step by Step*, Landau, Germany, 2021.

THE ANNALS OF "DUNAREA DE JOS" UNIVERSITY OF GALATI
FASCICLE IX. METALLURGY AND MATERIALS SCIENCE
N°. 2 - 2023, ISSN 2668-4748; e-ISSN 2668-4756
Article DOI: https://doi.org/10.35219/mms.2023.2.09

ADDITIVE MANUFACTURING THROUGH 3D PRINTING OF THE MARK HOS PIPE DN 50, USING ABS+ FILAMENT

Sorin Alexandru FICĂ[1], Claudiu BABIȘ[2], Andrei DIMITRESCU[2]
[1]ICPE-CA Bucuresti, Romania
[2]Politehnica University from Bucharest, Romania
e-mail: fica_sorin@yahoo.com, claudiubab8@gmail.com, andrei_dimitrescu@yahoo.com

ABSTRACT

This paper deals with the additive manufacturing by 3D printing of the Hose Pipe DN 50 landmark which is part of the Gas Reduction R2-Hose DN 2 in subassembly. This sub-assembly is a component part of the washing head of the light water well drilling installations FA 100, FA 125, FH 150 and FG 40. The generic name of the washing head will be FA 100. We use 3D printing technology because, on the one hand, it is technically possible to make the part and on the other hand, for economic reasons. It is approximately ten times cheaper to make the part through 3D printing than through conventional technologies

KEYWORDS: Hose pipe, 3D printing, Fused Deposition Modeling, water drilling installation

1. Introduction

Due to the common use of the washhead on light water well drilling rigs FA100, FA125, FH150 and FG40, its generic name will be "FA100 Washhead" [1-3].

The aim is to obtain the components of the washing head at water well drilling installations, through 3D printing additive manufacturing, both for technical and economic reasons [4-6]. From an economic point of view, it is approximately ten times cheaper to manufacture the parts of the washing head through 3D printing additive manufacturing than to manufacture them using conventional technologies. This issue represents a spectacular leap in work efficiency and productivity.

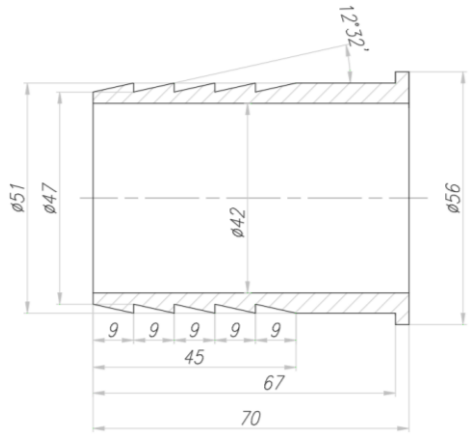

Fig. 1. *Execution drawing for Hose Pipe DN 50*

This paper deals with the additive manufacturing by 3D printing of the Hode Pipe DN 50 landmark, component part of the washing head of water well drilling installations, generically called FA 100.

The landmark Hose Pipe DN 50, whose additive manufacturing through 3D printing is to be described, is part of the Gas Reducer R2-Hose DN 2 subassembly.

THE ANNALS OF "DUNAREA DE JOS" UNIVERSITY OF GALATI
FASCICLE IX. METALLURGY AND MATERIALS SCIENCE
Nº. 2 - 2023, ISSN 2668-4748; e-ISSN 2668-4756
Article DOI: https://doi.org/10.35219/mms.2023.2.09

The landmark Hose Pipe DN 50 was manufactured by 3D FDM printing with ABS+ filament according to the drawing in Figure 1.

2. Fabrication

Figure 2 shows the 3D modeling in the Autodesk Fusion 360 program of the Hose Pipe DN 50 landmark, which results in the STL format file for slicing before its 3D printing.

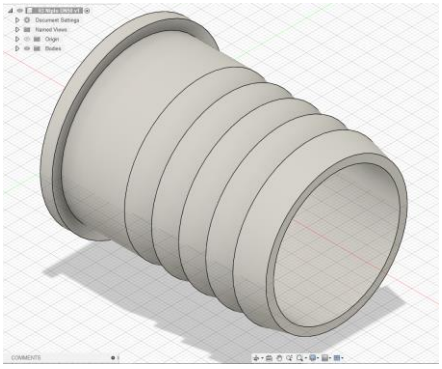

Fig. 2. *3D Modeling in the Autodesk Fusion 360 program of the Hose Pipe DN 50 landmark, which results in the STL format file for slicing" before its 3D printing*

Figure 3 shows the 3D slicing modeling of the Hose Pipe DN50 mm landmark, using the Ultimaker Cura 4.11 slicing program.

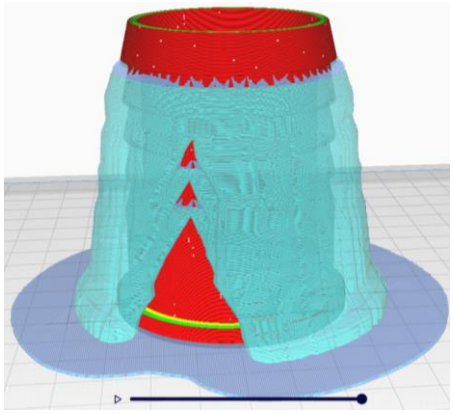

Fig. 3. *3D Slicing modeling of the Hose Pipe DN50 mm landmark, using the slicing program, Ultimaker Cura 4.11*

Figure 4 shows some of the settings for slicing the Hose Pipe landmark DN50 mm.

Other settings made for slicing the Hose Pipe DN50 mm are shown in Figure 5.

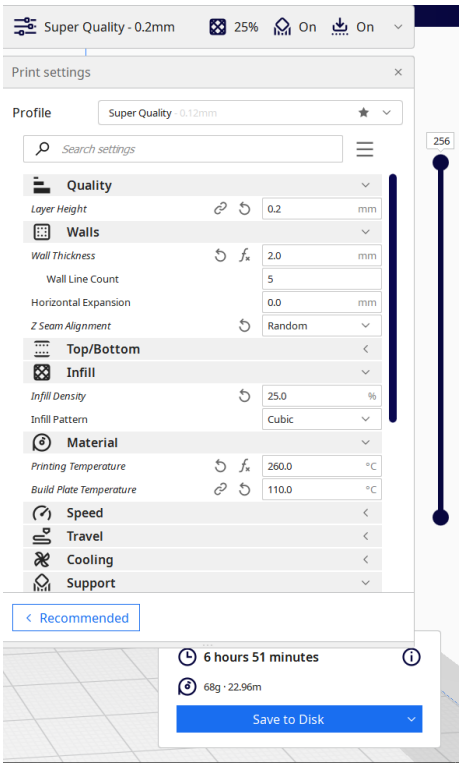

Fig. 4. *The first part of the settings for slicing the Hose Pipe landmark DN50 mm*

THE ANNALS OF "DUNAREA DE JOS" UNIVERSITY OF GALATI
FASCICLE IX. METALLURGY AND MATERIALS SCIENCE
Nº. 2 - 2023, ISSN 2668-4748; e-ISSN 2668-4756
Article DOI: https://doi.org/10.35219/mms.2023.2.09

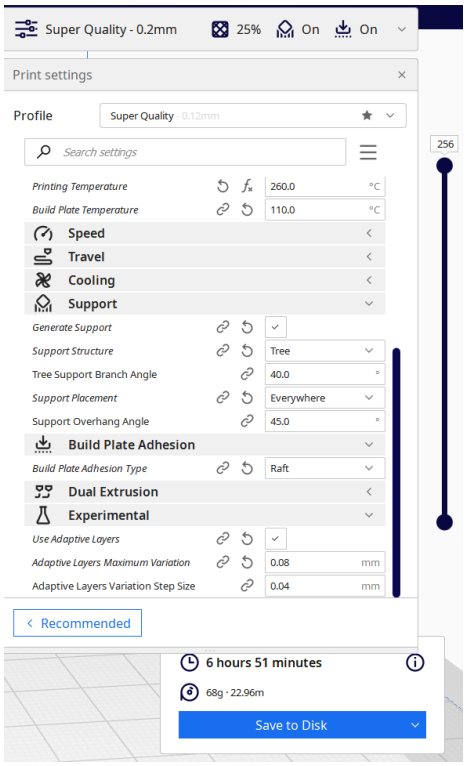

Fig. 5. *The second part of the settings for slicing the landmark HosePipe DN50 mm*

The main slicing settings for the Hose Pipe landmark DN50 mm in the Cura 4.13.1 program were as follows: Layer height = 0.2 mm; Wall thickness = 2 mm; Z-Seam Alignment = Random; Infill density = 25; Infill Pattern = Cubic; Material = ABS+ Printing Temperature = 260 ºC; Build Plate Temperature = 110 ºC; Generate Support = Yes; Support Structure = Tree; Tree Support Branch Angle = 40º; Support Placement = Everywhere; Support Overhang Angle = 39º; Build Plate Adhesion Type = Raft; Use Adaptive Layers = Yes; Adaptive Layers Maximum Variation = 0.08 mm; Adaptive Layers Variation Step Size = 0.04 mm.

It took 6 hours and 51 min to print the Hose Pipe DN50 mm and consumed 68 g of ABS+ filament. The Slice command is given.

Hose Pipe DN50 benchmark took 11 hours and 45 minutes to print. and consumed 67 g of ABS+ filament. The Slice command is given.

Figure 6 shows the landmark Hose Pipe DN50 mm, 3D printed, using ABS+ filament, on the Creality 3D printer, Ender 3 V2.

Fig. 6. *Landmark Hose Pipe DN50 mm fabricated by additive 3D printing on the Creality Ender 3 V2 3D printer*

THE ANNALS OF "DUNAREA DE JOS" UNIVERSITY OF GALATI
FASCICLE IX. METALLURGY AND MATERIALS SCIENCE
Nº. 2 - 2023, ISSN 2668-4748; e-ISSN 2668-4756
Article DOI: https://doi.org/10.35219/mms.2023.2.09

Conclusions

The manufacture of the landmark Hose Pipe DN50 mm through 3D printing, represented the optimal solution from a technical and economic point of view. In the conventional manufacturing version, a high manufacturing cost results and the labour productivity was low. In the 3D printed version made of ABS+ filament, the part costs approximately 10 times less, the labour being almost zero. This issue represents a spectacular leap in work efficiency and productivity.

This landmark is an integral part of the washing head from light water well drilling installations, type FA 100, FA 125, FH 150 and FG 40. The additive manufacturing by 3D printing of this landmark aims to reduce the manufacturing cost of light drilling installations water wells thus falling into the category of green projects and projects for the realization of industrial parts through additive methods.

The partial realization through additive manufacturing through 3D printing of some land-marks of light water well drilling installations has several advantages. On the one hand, from an economic point of view, the reduction of the manufacturing cost is obtained, and on the other hand, a modern, fast and relatively easy to implement technical solution is used.

Another objective pursued by the manufacture of light installations for drilling water wells at low costs and using modern technical solutions such as additive manufacturing through 3D printing, is the relaunch of irrigation in Romania. This is a requirement of the European commissioners in the National Recovery and Resilience Plan of Romania PNRR. The proposed solution is to make water wells with drilling installations, or a water well with a depth of 80 meters, on two hectares of land agricultural.

In the context of the war in Ukraine which led to the collapse of imports of raw materials and equipment in Europe and in the context of the container crisis in China, with delays of 2-3 years, for the import of equipment from China, it is possible to lay the foundations for an industrial relaunch and in Romania. Thus, it is proposed to align with the new reindustrialization of the EU by demonstrating the capability of manufacturing the prototype of the FH100 water well drilling installation, at the best price / quality ratio, by 3D printing and by manufacturing on CNC numerical control milling processing centers, with zero labour, this type of means of pro-duction having the status of Industrial Robots.

The objective pursued is the realization and testing of FH 100 type water well drilling installations, with hydraulic drive, on a monoaxle trailer, in a modern, flexible modular design, for the efficiency, flexibility and reduction of the energy costs of drilling, with 3 innovative modules being developed, namely: The module mechanically driven drilling head, Hydraulically driven Drilling Head Module and Hydraulic Drive Installation Module, integrated into the chassis of the monoaxle trailer These modules will contain innovative products of scientific and technological revolution consisting of resistance machine parts and other milestones made by manufacturing digitized additive, namely by 3D FDM printing, Fused Deposition Modeling, by hot extrusion layer by layer and by digitized subtractive manufacturing, by CNC processing.

At this moment, a true industrial, scientific and technological revolution is being dis-cussed worldwide, consisting in the development of Additive Manufacturing technologies through the use of 3D printing.

In this sense, the approach of manufacturing the components of light water well drilling installations, at the level of Romania, through additive methods such as 3D printing, is a perfectly justified technical-economic solution.

Acknowledgement

This work was carried out through the Nucleu Program within the National Research Development and Innovation Plan 2022-2027, implemented with the support of MCID, contract no. 42N/2023, project no. PN23140101.

We also thank the external collaborators from the Politehnica University of Bucharest.

References

[1]. Fica Sorin Alexandru, *Realizarea unei instalații inovative de foraj hidrogeologic cu acționare hidraulică a sistemului de manevră si acționare mecanică a capului de foraj de tip FA125*, Programul cercetare NUCLEU, 2017.

[2]. Fica Sorin Alexandru, *Additive manufacturing through 3D printing FDM-Fused Deposit Modeling of press bush*, Editura Academica Brâncuși, Târgu Jiu, ISSN 1844-640X, Fiability and Durability, no. 1, 2023.

[3]. Fica Sorin Alexandru, *Washing Head Housing, 3D printing from FA 100 drilling installation, using PETG fillament*, Editura Academica Brâncuși, Târgu Jiu, ISSN 1844-640X, Fiability and Durability, no. 1, 2023.

[4]. Zukas V., Jonas A. Zukas, *An Introduction in 3D Printing*, First Edition, Design Publishing Inc., 2015.

[5]. France A. K., *Make: 3D Printing, the Essential Guide to 3D Printers*, Maker Media, 2020.

[6]. J. Wild, *Fusion 360 Step by Step*, Landau, Germany, 2021.

MANUSCRISELE, CĂRŢILE ŞI REVISTELE PENTRU SCHIMB, PRECUM ŞI ORICE CORESPONDENŢE SE VOR TRIMITE PE ADRESA:

MANUSCRIPTS, REVIEWS AND BOOKS FOR EXCHANGE COOPERATION, AS WELL AS ANY CORRESPONDANCE WILL BE MAILED TO:

LES MANUSCRIPTS, LES REVUES ET LES LIVRES POUR L'ECHANGE, TOUT AUSSI QUE LA CORRESPONDANCE SERONT ENVOYES A L'ADRESSE:

MANUSCKRIPTEN, ZIETSCHRITFTEN UND BUCHER FUR AUSTAUCH SOWIE DIE KORRESPONDENZ SID AN FOLGENDE ANSCHRIFT ZU SEDEN:

After the latest evaluation of the journals by the National Center for Science Policy and Scientometrics (**CENAPOSS**), in recognition of its quality and impact at national level, the journal will be included in the B^+ category, 215 code (http://cncsis.gov.ro/userfiles/file/CENAPOSS/Bplus_2011.pdf).

The journal is already indexed in:

DOAJ: https://doaj.org/

SCIPIO-RO: http://www.scipio.ro/web/182206

EBSCO: http://www.ebscohost.com/titleLists/a9h-journals.pdf

Google Academic: https://scholar.google.ro

Index Copernicus: https://journals.indexcopernicus.com

Crossref: https://search.crossref.org/

The papers published in this journal can be viewed on the website: http://www.gup.ugal.ro/ugaljournals/index.php/mms

Name and Address of Publisher:
Contact person: Prof. Dr. Eng. Elena MEREUȚĂ
Galati University Press - GUP
47 Domneasca St., 800008 - Galati, Romania
Phone: +40 336 130139
Fax: +40 236 461353
Email: gup@ugal.ro

Name and Address of Editor:
Ș. L. Dr. Eng. Marius BODOR
"Dunarea de Jos" University of Galati, Faculty of Engineering
111 Domneasca St., 800201 - Galati, Romania
Phone: +40 336 130208
Phone/Fax: +40 336 130283
Email: marius.bodor@ugal.ro

AFFILIATED WITH:

- THE ROMANIAN SOCIETY FOR METALLURGY
- THE ROMANIAN SOCIETY FOR CHEMISTRY
- THE ROMANIAN SOCIETY FOR BIOMATERIALS
- THE ROMANIAN TECHNICAL FOUNDRY SOCIETY
- THE MATERIALS INFORMATION SOCIETY (ASM INTERNATIONAL)

Edited under the care of the FACULTY OF ENGINEERING

Annual subscription (4 issues per year)

Fascicle DOI: https://doi.org/10.35219/mms

Volume DOI: https://doi.org/10.35219/mms.2023.2

Editing date: 15.06.2023
Number of issues: 200
Printed by Galati University Press (accredited by CNCSIS)
47 Domneasca Street, 800008, Galati, Romania